HHS Public Access

Author manuscript

Cancer Res. Author manuscript; available in PMC 2024 June 15.

Published in final edited form as:

Cancer Res. 2023 December 15; 83(24): 4095–4111. doi:10.1158/0008-5472.CAN-23-2729.

Genome-Wide CRISPR Screens Identify Multiple Synthetic Lethal Targets That Enhance KRAS^{G12C} Inhibitor Efficacy

Suman Mukhopadhyay[1,^,*], **Hsin-Yi Huang**[1,*], **Ziyan Lin**[2,+], **Michela Ranieri**[1,+], **Shuai Li**[1,+], **Soumyadip Sahu**[1], **Yingzhuo Liu**[1], **Yi Ban**[1], **Kayla Guidry**[1], **Hai Hu**[1], **Alfonso Lopez**[1], **Fiona Sherman**[1], **Yi Jer Tan**[1], **Yeuan Ting Lee**[1], **Amanda P. Armstrong**[1], **Igor Dolgalev**[1], **Priyanka Sahu**[1], **Tinghu Zhang**[3], **Wenchao Lu**[3], **Nathanael S. Gray**[3], **James G Christensen**[4], **Tracy T. Tang**[5], **Vamsidhar Velcheti**[1], **Alireza Khodadadi-Jamayran**[2], **Kwok-Kin Wong**[1,^], **Benjamin G. Neel**[1,^]

[1]Laura and Isaac Perlmutter Cancer Center, NYU Grossman School of Medicine, NYU Langone Health, New York, United States

[2]Applied Bioinformatics Laboratories, Office of Science and Research, New York University Grossman School of Medicine, New York, United States

[3]Department of Chemical and Systems Biology, ChEM-H, Stanford Cancer Institute, School of Medicine, Stanford University, California, United States

[4]Mirati Therapeutics, Inc., San Diego, California, United States

[5]Vivace Therapeutics, Inc., San Mateo, California, United States

Abstract

Non-small lung cancers (NSCLCs) frequently (~30%) harbor *KRAS* driver mutations, half of which are *KRAS*^{G12C}. *KRAS*-mutant NSCLC with co-mutated *STK11* and/or *KEAP1* is particularly refractory to conventional, targeted, and immune therapy. Development of KRAS^{G12C}

[^]**Corresponding authors:** Benjamin G. Neel, Department of Medicine, Perlmutter Cancer Center, New York University Grossman School of Medicine, 522 First Avenue, New York, NY 10016. Phone: 212-263-3019; Fax: 212-263-9190; benjamin.neel@nyulangone.org; Kwok-Kin Wong, Division of Hematology and Medical Oncology, Department of Medicine, Perlmutter Cancer Center, New York University (NYU) Grossman School of Medicine, NYU Langone Health, 550 1st Ave, Smilow 1011 New York, NY 10016; Phone: (212) 263-9203; kwok-kin.wong@nyulangone.org; Suman Mukhopadhyay, Department of Medicine, Perlmutter Cancer Center, New York University Grossman School of Medicine, 522 First Avenue, Smilow 707, New York, NY 10016. Phone: 917-664-5682; suman.biology@gmail.com, suman.mukhopadhyay@nyulangone.org.

[*]Contributed equally

[+]Contributed equally

AUTHORS' CONTRIBUTIONS

S. Mukhopadhyay: Conceptualization, data curation, formal analysis, supervision, validation, investigation, visualization, methodology, writing–initial draft, project administration, writing–review and editing.

H. Huang: Conceptualization, resources, validation, investigation.

Z. Lin: Data curation, software, formal analysis, visualization.

M. Ranieri- Conceptualization, resources, validation

S. Li- Conceptualization, resources, investigation

S. Sahu, Y. Liu, Y. Ban, K. Guidry, H. Hu: Validation, resources, investigation

A. Lopez, F. Sherman, Y. Tan, Y. Lee, A.P. Armstrong, I. Dolgalev, P. Sahu, T. Zhang, W. Lu, N. Gray, J. Christensen, T.T. Tang, V. Velcheti: Resourses

A. Khodadadi-Jamayran: Data curation, software, formal analysis, visualization.

K.-K. Wong: Conceptualization, resources, data curation, supervision, funding acquisition, methodology, project administration, writing–initial draft, writing– review and editing.

B.G. Neel: Conceptualization, resources, data curation, supervision, funding acquisition, methodology, writing–final draft, project administration, writing–review and editing.

inhibitors (G12Cis) provided a major therapeutic advance, but resistance still limits their efficacy. To identify genes whose deletion augments efficacy of the G12Cis adagrasib (MRTX-849) or adagrasib plus TNO155 (SHP2i), we performed genome-wide CRISPR/Cas9 screens on *KRAS/STK11*-mutant NSCLC lines. Recurrent, potentially targetable, synthetic lethal (SL) genes were identified, including serine-threonine kinases, tRNA-modifying and proteoglycan synthesis enzymes, and YAP/TAZ/TEAD pathway components. Several SL genes were confirmed by siRNA/shRNA experiments, and the YAP/TAZ/TEAD pathway was extensively validated *in vitro* and in mice. Mechanistic studies showed that G12Ci treatment induced gene expression of RHO paralogs and activators, increased RHOA activation, and evoked ROCK-dependent nuclear translocation of YAP. Mice and patients with acquired G12Ci- or G12Ci/SHP2i-resistant tumors showed strong overlap with SL pathways, arguing for the relevance of the screen results. These findings provide a landscape of potential targets for future combination strategies, some of which can be tested rapidly in the clinic.

Keywords

KRAS G12C; Resistance; CRISPR screen; YAP/TEAD

INTRODUCTION

The most common subtype of lung cancer, non-small cell lung cancer (NSCLC), is a leading cause of cancer-associated morbidity and mortality worldwide. Mutations in *KRAS* drive 25-30% of NSCLC cases (1–3); approximately half of these mutations convert glycine 12 to cysteine (G12C). Concomitant mutation or deletion (hereafter, “co-mutations”) of different tumor suppressor genes (e.g., *TP53*, *SMARCA4*, *STK11*, and/or *KEAP1*) typically occur in concert with *KRAS* mutations (4,5). *KRAS* mutations also occur frequently in other tumors, including colorectal cancer (CRC) and pancreatic adenocarcinoma (PDAC). The specific *KRAS* allele, as well as other co-occurring genomic abnormalities, differ in these neoplasms, with $KRAS^{G12C}$ comprising only ~5% of CRC-associated *KRAS* mutations and 1-3% of PDAC cases. Tumor properties, including therapy response, are determined by the specific combination of driver and tumor suppressor gene alterations and the cell-of-origin of the tumor. In NSCLC, for example, *STK11* and/or *KEAP1* mutations are associated with poor response to conventional, targeted, and immune therapies (5–7). The lack of effective treatment strategies for this subgroup represents a major unmet medical need.

KRAS had long been viewed as “undruggable”. The recent development of small molecule covalent G12C inhibitors (G12Cis) represents a triumph of chemical biology and drug design. Several G12Cis (6,8) are in clinical trials, and two, sotorasib (AMG-510) and adagrasib (MRTX-849), are FDA-approved for second-line treatment of $KRAS^{G12C}$ NSCLC. While these drugs clearly have clinical activity, overall response rates (30-40%) and disease control (~60%) in NSCLC are modest and transient, with median duration less than one year (9,10). Response rates in $KRAS^{G12C}$-mutant CRC are even lower (11).

Multiple mechanisms of intrinsic and acquired resistance (10,12,13), have been identified; hence, drug combinations will likely be needed to maximize the clinical efficacy of

G12Cis (and probably other, emerging KRAS inhibitors) in NSCLC and other diseases. For example, combinations of G12Ci and SHP2 inhibitors (SHP2i) such TNO155 (14) and RMC-4550 (15) have been validated pre-clinically and are now being explored in the clinic (NCT04699188, NCT05480865).

To more globally define the landscape of potential combination strategies, we used genome-wide CRISPR/Cas9 screening to identify genes whose inactivation enhances the efficacy of MRTX-849 alone or in combination with TNO-155 in four *KRAS*^{G12C}-mutant NSCLC cell lines. Owing to the association of these genotypes with poor therapeutic response, we chose lines with co-mutations in *STK11*; three were also *KEAP1*-defective. Our results credential TEAD inhibition as a potential strategy for enhancing adagrasib (and likely sotorasib) response and identify multiple other potentially "druggable" targets for combination therapy.

MATERIALS AND METHODS

Cell Lines and Reagents

MIAPaCa-2, Calu-1, H23, H358, H2030, H2122, HCC44, SW1463, and SW837 cells were obtained from laboratory inventories, acquired as reported previously (16). The KCL cell line was derived following an established protocol (17). Briefly, nodules were harvested from lungs with visible tumors in Ad-Cre-induced, *KRAS*$^{LSL\text{-}G12C/+}$; *Stk11*$^{flox/flox}$ (KCL) mice on C57BL/6J background (generated as described below) and minced in RPMI 1640 containing 10% Fetal Bovine Serum (FBS, Sigma-Aldrich), 1X GlutaMAX Supplement (Gibco, Cat#: 35050061) and 1x Antibiotic-Antimycotic (Gibco, Cat#: 15240062). The media were exchanged daily, and cells were cultured for at least five passages to establish a stable cell line.

All cultures were maintained at 37°C in a 5% CO_2 environment using the media conditions specified by the supplier or the originating laboratory. Once thawed, aliquots of cell lines were maintained for no longer than 3 months. TET-ON-shRNA stable cell lines (see below) were cultured in tetracycline-free FBS (Takara Bio). Lines were tested for mycoplasma contamination by PCR 5-7 days after thawing.

MRTX-849 was provided by Mirati Therapeutics under a collaborative research agreement. TNO155, Y27632, and VRK-IN-1 were purchased from MedChemExpress. VT104 and VT106 were provided by Vivace Therapeutics under a collaborative MTA. MYF-03-176 was kindly provided by Dr. Nathanael S. Gray, Stanford University, under a collaborative MTA. SHP099 was purchased from WuXi AppTec (Shanghai) Co., Ltd.

Plasmids, si/shRNAs, and Lentivirus Generation

To induce *TEAD1* (VB230130-1327fbp/VectorBuilder) or *WWTR1/TAZ* (VB230411-1009nze/VectorBuilder) (over)expression in KCL cells, expression plasmids were generated that fuse the respective coding sequences to 3X-flag tags. These plasmids and a control vector (VB900120-7563srw) were obtained from VectorBuilder. The following constructs were obtained from Addgene: pLX304 (#25890), *YAP1* (#42555), *YAP1*^{S6A} (#42562), and *YAP1*^{S94A} (#59145), dominant negative *TEAD* and cognate vector control (pInducer20 EGFP-TEADi, #140145, and pInducer20 #44012), and 8xGIITC-luciferase

(#34615) and Renilla luciferase (#27163). Stable cell lines overexpressing the indicated genes were generated using lentiviral gene transduction (17).

Doxycycline (Dox)-inducible gene knockdowns were achieved by using TET-ON lentiviral vectors (Tet-pLKO-Puro backbone, Addgene #21915) expressing the appropriate targeting shRNA and a puromycin resistance gene (pLKO-Tet-On-Gene –shRNA1 and –shRNA2). A non-targeting shRNA vector (pLKO-Tet-On-shRNA-Control) served as control. Stable lines were established by puromycin selection for 7 days, and shRNAs were induced by adding Dox (1 μg/ml) to the culture medium. Suggsted sequences for shRNAs were obtained from the Broad Institute of MIT and were designated *TEAD1* #1 (TRCN0000015799), *TEAD1* #2 (TRCN0000015800), *ELP3* #1 (TRCN0000001280), *ELP3* #2 (TRCN0000235508), *ELP5* #1 (TRCN0000130483), *ELP5* #2 (TRCN0000127506), *RIOK2* #1 (TRCN0000197250), and *RIOK #2* (TRCN0000196684).

To generate lentiviruses, HEK-293T cells were co-transfected with lentiviral constructs and the packaging plasmids psPAX2 (Addgene, #12260) and pMD2.G (Addgene, #12259) using Lipofectamine 3000 (Invitrogen, Cat#: L3000008) according to the manufacturer's instructions. After 48h, culture media were passed through a 0.45 μm filter (Corning, cat#: 431225) to remove cell debris, and supernatants containing viral particles, supplemented with 8 μg/ml of polybrene (Fisher Scientific, cat#: TR1003G), were used to infect 70% confluent cells in 6-well plates for 16h at 37 °C.

For siRNA experiments, cells were plated in 6-well plates at 30% confluence in medium containing 10% FBS. After 24 hr, cells were transfected with siRNA (100 nM) using Lipofectamine RNAiMAX according to the manufacturer's instructions. After 6 hr, media were replaced. *TEAD1* (L-012603-00-0005), *RIOK2* (L-005002-00-0005), ELP5 (L-017992-00-0005), *VRK1* (L-004683-00-0005), *WWTR1* (L-016083-00-0005) and *ELP3* (L-015940-01-0005) siRNAs were obtained from Horizon Discovery.

CRISPR/Cas9 Screens

Two separate batches of each cell line were transduced with the TKOv3 CRISPR KO lentivirus library (18) at a low MOI (~0.3). Two days post-infection, the media were supplemented with puromycin, and cells were selected for 8 days. Following a recovery phase, a 500X library representation of infected cells from each batch was treated with DMSO (vehicle) or MRTX-849 at twice the IC50 for each line for 8 doubling periods. For combination screens, TN0155 was applied at the IC50 dosage or at 3 μM if the IC50 for the cell line exceeded that value. Screens with TNO155 alone used the same concentration of SHP2i as the combination screens. Upon screen conclusion gDNA was extracted and amplified via PCR, as described (19). The final PCR products were sequenced using an Illumina NovaSeq 6000 (SP 100 Cycle Flow Cell v1.5), and sequencing results were analyzed using MaGeCK (20). Downstream statistical analyses and plot generations were performed in R environment (4.0.3). Pathway analysis were generated by Enrichr (21). Gene set enrichment analysis was obtained by deploying GSEA software (22). CIRCOS plots were generated by using Metascape (23).

Cell Viability and Proliferation Assays

Cells were seeded in 96-well plates (1,000–2,000 cells/well) and treated with drugs at the indicated concentrations for the indicated times (3-7 days). Media (including inhibitors) were replaced every two days. Dose-response curves were generated using the MTS-based Cell Counting Kit-8 (CCK8) assay (Enzo, ALX-850-039-KI02). Three hours after addition of CCK-8 reagent to cells, A_{450} was recorded using a FlexStation 3 multi-mode microplate reader according to the manufacturer's instructions. IC50s were calculated with GraphPad Prism. For all other proliferation assays, cells were harvested and stained with trypan blue (# T8154, Sigma-Aldrich), and viable (trypan blue-excluding) cells were quantified with a Countless II automated cell counter (Invitrogen). Drug interaction between MRTX-849 and VT104 was assessed by Bliss analysis using the formula: $Y_{ab,P} = Y_a + Y_b - Y_a Y_b$, where Y_a stands for percentage inhibition of drug a and Y_b stands for percentage inhibition of drug b. Synergy was defined as % observed effect > $Y_{ab,P}$ (24).

RNA Extraction and RT-qPCR

Total RNA was extracted from cell pellets using the RNeasy Plus Mini Kit (QIAGEN, Cat#: 74136) and reverse transcribed using the High-Capacity RNA-to-cDNA™ Kit (Thermo Fisher Scientific, Cat#: 4387406) as per the manufacturers' protocols. cDNAs were diluted and analyzed by RT-qPCR using PowerUp™ SYBR™ Green Master Mix (Thermo Fisher Scientific, Cat#: A25742). PCR amplification and detection were achieved by using the QuantStudio 3 Real-Time PCR System (Applied Biosystems) and *CYR61*-specific primers (F-CYR61: CTCGCCTTAGTCGTCACCC; R-CYR61: CGCCGAAGTTGCATTCCAG), *VRK1*-specific primers (F-VRK1: CCAACGAGCTGCAAAACC; R-VRK1: TGTCATGTAGACCAGACCCCC). *CYR61* and *VRK1* levels were normalized to those of *ACTB* and represented as fold-change in gene expression in the test sample relative to the control.

Bulk RNA-seq and RPPA

Bulk RNA-seq was performed on total RNA from cell lines or isolated tumor cells by the PCC Genome Technology Center Shared Resource (GTC). Libraries were prepared with the Illumina TruSeq Stranded Total RNA Sample Preparation Kit and sequenced on an Illumina NovaSeq 6000 platform utilizing 150-bp paired end reads. Sequencing data were de-multiplexed and transformed into FASTQ format by using Illumina bcl2fastq software. Subsequent data processing and analysis were performed by the PCC Applied Bioinformatics Laboratories (ABL). Reads were adapter- and quality- trimmed using Trimmomatic before alignment with the human or mouse genome using the splice-aware STAR aligner. Using featureCounts (25), counts for each gene were created based on the number of aligned reads overlapping its exons. These counts were standardized and subsequently evaluated for differential expression via the DESeq2 R package, using negative binomial generalized linear models. Lastly, the Enrichr tool was employed for pathway analysis of the bulk RNA-seq data.

RPPA for isolated tumor cells were performed at the MDACC Functional Proteomics core facility as described (26). Standardized intensity data were log 2-transformed, and heat maps

were row-normalized using Z score. Rows and columns were clustered via hierarchical clustering as described (26).

Luciferase Assays

H2030 cells in 6-well plates were transiently co-transfected with 8xGTIIC-luciferase (2 μg) and Renilla luciferase (200 ng) plasmids, using X-tremeGENE HP DNA Transfection Reagent (Sigma). Luciferase activity was measured with the Dual-Glo Luciferase Assay System (Promega). To control for transfection efficiency, firefly luciferase activity was normalized to Renilla luciferase readings. Experiments were performed three times.

RHOA Activity Assays

RHOA activity (RHO-GTP) was quantified by using a G-LISA activation assay kit (Cytoskeleton), following the manufacturer's guidelines. Briefly, cells were lysed using a buffer supplied in the kit, and extracts were transferred to 96-well plates layered with GST-RHOA binding domain fusion protein. After incubation with gentle shaking at 4°C for 30 min., plates were washed three times with "wash buffer" prior to the addition of "antigen-presenting buffer" (each from Cytoskeleton) containing anti-RHOA primary monoclonal antibody for 30 min., washed 3 times, incubated with horseradish peroxidase (HRP)–linked secondary antibodies and quantified by using a FlexStation 3 multi-mode microplate reader.

Immunofluorescence

Cells (2×10^3/well) were seeded in 8-well chamber slides (Nunc Lab-Tek, Thermo Fisher), allowed to grow overnight in complete medium (RPMI with 10% FBS and 1X penicillin/streptomycin), and treated with MRTX-849 for the times indicated. Cells were then fixed in 4% paraformaldehyde for 10 minutes at room temperature, rinsed three times for 5 min. each in PBS, and permeabilized in 0.1% Triton X-100/5% FBS in PBS for a 1 hr at RT. Following blocking, slides were incubated with monoclonal anti-YAP1 antibody (Cell Signaling, Cat# 14074, 1:100 in 5% FBS/PBS) at 4°C overnight, washed four times with PBS, incubated with Alexa Fluor Plus 488 (Thermo Fisher Scientific, Cat#: A-11001, 1:400 dilution) secondary antibodies for 2 hr, and washed three times with PBS. Nuclei were stained with DAPI (BioLegend, Cat#: 422801) for 5 min, and slides were washed two more times in PBS before mounting with Fluorescence Mounting Medium (Dako, Cat#: S3023). Images were acquired with a Zeiss 880 Laser Scanning Confocal Microscope (Axio Observer) equipped with Zen 3.0 software (ZEN blue, Carl Zeiss Inc.) and were processed by Fiji software (NIH).

YAP localization in cell populations was quantified by two double-blinded observers. Partial nuclear, total nuclear, and total cytosolic localization of YAP were defined using control immunofluorescence images. Then, all cells were scored independently and blindly into one of these categories. YAP and DAPI channels were merged using ImageJ, and total cell count (at least 50 cells per group) as well as the number of cells scored based on each pattern of YAP localization were generated using the multi-point function in ImageJ. Raw data sets were averaged, and the proportion of cells in each staining category was determined. The results of the two double-blinded observers were averaged and displayed as bar plots.

Significance was evaluated by ANOVA with Tukey's correction for multiple comparisons. All analyses were performed using GraphPad Prism.

Immunoblotting

Cells were washed twice with ice-cold PBS, scraped into 700 ml PBS, and centrifuged at 1500 x r.p.m. for 5 min. Pellets were lysed in RIPA buffer (ThermoFisher Scientific #89900) with a protease and phosphatase inhibitor cocktail (ThermoFisher Scientific #78440). Protein concentrations were determined using a BCA protein assay kit (ThermoFisher Scientific #23225) with bovine serum albumin as the protein standard. Total cellular protein (30 μg) was boiled in 6x SDS sample buffer (Boston BioProducts cat# BP-111R), resolved on 4-20% Mini-PROTEAN TGX SDS-PAGE gels (Bio-Rad, Cat # 4568095, 5678095 and 5671094), and transferred to nitrocellulose. Membranes were blocked with TBS buffer (LI-COR, Cat # 927-60001), incubated with primary antibodies overnight at 4°C and secondary antibodies for 1 hour at room temperature, and visualized by using an Odyssey classic infrared imaging system (LI-COR) and Image Studio Lite (V 5.2).

Antibodies used for immunoblots were as follows: monoclonal anti-β-actin (# A5441; 1:10,000) and anti-FLAG (#F1804; 1:5,000) from Sigma; monoclonal anti-β-actin (#4970S), anti-GAPDH (#5174S; 1:5000), anti-TEAD1 (#12292; 1:1000), anti-ELP3 (#5728S; 1:1000), anti-TAZ (#72804;1:1000), and monoclonal anti-GFP (#2956; 1:1000), all from Cell Signaling; polyclonal anti-RIOK2 (Abcam #Ab88485; 1:1000), polyclonal anti-ELP5 (Protein Tech #10162-1-AP; 1:500), and IRDye 680RD donkey anti-Mouse IgG (#925-68072), IRDye 800CW donkey anti-rabbit IgG (#925-32212), IRDye 680RD donkey anti-Rabbit IgG (#926-68073), and IRDye 800CW donkey anti-Mouse IgG (# 925-32212), all from LICOR.

Genetically Engineered Mouse Model (GEMM) Generation and Treatment

All animal studies were approved by the Institutional Animal Care and Use Committee at New York University Grossman School of Medicine and adhered to the guidelines stipulated in the Guide for the Care and Use of Laboratory Animals. *Kras*$^{LSL-G12D/+}$; *Stk11*$^{flox/flox}$ (KdL) (27) and *KRAS* $^{LSL-G12C/+}$ (KC) (28) mice were described previously. These mice were inter-crossed to generate *KRAS*$^{LSL-G12C/+}$;*Stk11*$^{flox/flox}$ (KCL) progeny, all on C57BL6/J background. Mice of both sexes were used for experiments, and age- and sex-matched animals were grouped randomly. Ad-Cre virus (1×10^7 PFU) as instilled nasally at 7–8 weeks of age, and mice were monitored for tumor development by magnetic resonance imaging (MRI). KCL tumor-bearing mice were dosed by gavage with MRTX-849 (100mg/kg), alone or in combination with SHP099 (75mg/kg), on a 5 days on/2 days off schedule. Tumor development was monitored by MRI every 2 weeks (see below). After 3-6 months of treatment, tumors were harvested and cut into pieces for RNA-seq and RPPA analysis.

For syngeneic tumor experiments, KCL cells (10^6 in 200 μl PBS) were injected subcutaneously into the right flanks of male C57BL/6J mice (Jackson Laboratory). For xenografts, H2030 cells (5×10^6) were injected subcutaneously into the right flanks of *Crl:NU-Foxn1nu/nu* mice (Charles River, #088) with a 1:1 mixture of cell suspension

in Matrigel (Corning, Cat#354234). When tumor volumes reached ~100 mm^3 (for syngeneic grafts) or ~300 mm^3 (for xenografts), mice were randomized to the following groups: vehicle control, MRTX-849 (100 mg/kg/d), VT104 (10 mg/kg/d), and MRTX-849 (100mg/kg/d) and VT104 (10 mg/kg/d). Mice were weighed two times a week prior to dosing and throughout the study. Tumors were measured in 2 dimensions (length and width) twice a week and volumes (mm^3) were calculated as (length ×$width^2$)/2).

MRI Quantification

For magnetic resonance imagining (MRI) of the lung fields, mice were anesthetized with isoflurane, and 16 consecutive sections were scanned using a BioSpec USR70/30 horizontal bore system (Bruker). Tumor volumes in whole lungs were quantified using 3-D slicer software. Acquisition of MRI signals was adapted to cardiac and respiratory cycles to minimize motion effects during imaging.

scRNA-Seq of Patient Samples

Human lung tumor specimens were collected from patients at New York University Langone Hospital (New York, NY) with patient written informed consents and the approval from the Institute Research Ethics Committee and with the approval of the Institutional Review Board, in accordance with the Declaration of Helsinki, CIOMS, Belmont Report, and U.S. Common Rule.

scRNAseq was performed on cells from fresh tumor biopsies from patients with $KRAS^{G12C}$-mutant NSCLC treated with AMG-510 (sotorasib) or MRTX-849 (adagrasib)/TNO155 or from a control $KRAS^{G12V}$-mutant tumor. Tumor samples were mechanically and enzymatically digested using Collagenase 1000X and DNase for 15-30 min at 37°C. Single cells were passed through a 70 μm filter, and red blood cells were lysed in ACK buffer. Cells were counted with trypan blue, stained with 0.1 uM Calcein (final concentration) for 20 min at 37°C at a final cell concentration of ~10^6 cells/ml, amd resuspended in media containing DAPI (1:1000 of 1 mg/mL stock). Single cells in 0.04% BSA solution in PBS were recovered by FACS (PCC Immune Monitoring Laboratory) and subjected to 10X Genomics scRNAseq library prep and sequencing. Raw sequencing files were mapped to the reference genome (hg38), and gene-cell matrices were generated by 10x Genomics Cell Ranger software (v 3.1.0). Matrices from different samples were merged and imported into Seurat (v 4.1.3). Quality controls included calculating the number of genes, UMIs, and the proportion of mitochondrial genes for each cell. Cells with a low number of covered genes (gene count < 500) or high mitochondrial counts (mt-genes > 0.2) were filtered. Log-normalization was performed on the filtered matrix, Principal Component Analysis (PCA) was performed, and the top 20 PCs were used as input for Uniform Manifold Approximation and Projection (UMAP) and graph-based clustering. Marker genes were used to determine tumor cell types. All downstream statistical analyses and plot generation were performed in R environment (4.0.3).

Statistical Analysis

Data are expressed as mean ± standard deviation. Significance was assessed using Student's t-test, or 1-way ANOVA with Tukey's multiple comparisons test, as appropriate. Statistical

analyses were performed in Prism 10 (GraphPad Software). Significance was set at P = 0.05 for all analyses except screen data, where genes with FDR<0.1 were considered for further analysis. P values and FDRs for individual experiments are stated in the text and/or figure legends.

Data Availability

All the raw sequencing reads, processed files, and metadata are deposited in Gene Expression Omnibus with the accession number GSE240120. All other data supporting the findings of this study are available from the corresponding authors upon request.

RESULTS

Genome-Wide CRISPR/Cas9 Screens Identify G12Ci Synthetic Lethal Genes

To search for genes that afffect G12Ci efficacy, we performed pooled genome-wide CRISPR/Cas9 “dropout” screens on four *KRAS*^{G12C}-mutant NSCLC lines co-mutant/deleted for *STK11*; three (excluding H23) also have *KEAP1* mutations (Supplementary Fig. 1A). Notably, *KRAS*^{G12C}-mutant NSCLC with *KEAP1* and possibly *STK11* mutations are more resistant to single-agent G12Ci treatment, as well as conventional chemoradiation and immune therapy (6,29,30). Cells from each line were transduced with the TKOV3 lentiviral CRISPR library, which targets 18,053 protein-coding genes with sgRNA RNAs per gene (18,31), at an M.O.I of 0.3 and 500X representation for each sgRNA. Infected cells were cultured for eight population doublings in vehicle (DMSO) or with MRTX-849(adagrasib) added at twice the IC_{50} concentration (2 x IC50) for each line (Fig. 1A; Supplementary Fig. 1B). Genomic DNA (gDNA) was sequenced, and gene “dropout” was assessed by robust rank aggregation, as implemented in MaGeCK (20). Log_2 fold-changes were calculated and displayed as volcano plots (Fig. 1B; Supplementary Table S1). Biological replicates were strongly correlated, indicating that the screens were high-quality (Supplementary. Fig. 1C).

Shared and unique synthetic lethal (SL) genes were identified in the four lines (Fig. 1C; Supplementary Table 2). More than 40 genes were depleted (FDR<0.1) in at least three lines (Fig. 1D); even more (~330) “dropped out” in at least two (Supplementary Table 2). Heterogeneity at the gene level probably reflects other genetic/epigenetic changes in these lines (in addition to *KRAS*, *STK11*, and KEAP1). *SHOC2*, a known SL gene in MEK-inhibitor treated cells (32), was depleted in 3/4 lines, as were genes encoding several enzymes that might be targeted therapeutically, including three serine/threonine kinases (*VRK1*, *RIOK2*, *PKN*), multiple components of the elongator complex (*ELP2*, *ELP3*, *ELP4, ELP5*), metabolic genes (*PGD*, *PGM3*), and genes (*EXT1*, *EXT2*) involved in heparan sulfate biosynthesis, among others. Enrichr analysis revealed SL pathways (p<0.05) shared in at least two lines, with most common to three or four (Fig. 1E). Several of these (colored red) were expected based on knowledge of the RAS pathway and inhibitor effects (33,34), including MAPK Family Signaling, PI3K/AKT/mTOR Signaling, FGF Signaling, PDGF Signaling, Autophagy, C-MYC Pathway and E2F targets. Others included potential novel, parallel targets, including DNA damage (Fanconi anemia pathway), heparan sulphate metabolism, glycosylation, and translation initiation pathways (colored black). Genes belonging to the Hippo (YAP/TAZ) pathway (colored blue) were enriched in dropouts

from 3/4 lines; moreover, *TEAD1* and *WWTR1* (encoding TAZ) were each SL in two lines, while *YAP1* showed significant dropout in H2030 (Fig. 1D and 1E; Supplementary Table S2).

YAP1/TAZ/TEAD Inhibition Enhances Adagrasib Action

TEAD inhibitors are in clinical trials for *NF2*-mutant mesothelioma and other indications (e.g., NCT05228015 and NCT04665206) (35). YAP/TAZ pathway activation is also a known mechanism of resistance to other targeted therapies, including RAF^{V600E} and MEK inhibitors (36). Comporting with the screen results, *TEAD1* or *WWTR1* depletion by siRNAs (“Smartpool”) or doxycycline-inducible shRNAs enhanced MRTX-849 efficacy in multiple lines (Fig. 2A and B; Supplementary Fig. 2A-B). Expressing a dominant negative *TEAD1* mutant (37) had similar effects (Fig. 2C; Supplementary Fig. 2C). Conversely, overexpression of *TEAD1* (Fig. 2D; Supplementary Fig. 2D), *WWTR1* (Fig. 2E; Supplementary Fig. 2E), *YAP1* (Fig. 2F; Supplementary Fig. 2F), or a constitutively active, nucleus-restricted form of *YAP1* (38), YAP^{S6A} (Fig. 2G; left panel; Supplementary Fig. 2G) in “KCL” cells (derived from $KRAS^{G12C}$;*Stk11*−/− mice; see Methods) caused drug resistance. By contrast, YAP^{S94A}, which encodes a mutant unable to associate with TEAD family members (39), did not affect MRTX-849 response (Fig. 2G, right panel, Suppl Fig. 2G). Collectively, these findings indicate that YAP1 and/or TAZ, acting in the nucleus by binding TEAD1 (or other TEAD family members), can antagonize G12Ci action and cause resistance.

RHO Directs ROCK-Dependent Nuclear Localization of YAP in Response to MRTX-849

We next asked whether YAP/TAZ/TEAD activity is modulated by G12Ci treatment. H2030 cells were transiently transfected with 8XGTIIC-Luci, a luciferase reporter driven by TEAD binding sites, and exposed to MRTX-849 (IC50 dosage for 48 hours) or left untreated. Notably, TEAD reporter activity increased by >6-fold in G12Ci-treated cells (Fig. 3A). Moreover, transcript levels of the YAP/TEAD-inducible gene *CYR61* were increased after 48h of MRTX-849 treatment in two NSCLC lines tested (Supplementary Fig. 3A). To assess the global effects of G12Ci treatment on the NSCLC transcriptome, we performed RNAseq on two MRTX-849-treated H2030 and H2122 cells. Unsupervised clustering clearly separated control and treated groups in both lines (Fig. 3B, Supplementary Table S3). Remarkably, many upregulated pathways, including Hippo Signaling, conformed to the SL pathways identified by our screen (compare Fig. 1E and 3C).

YAP/TAZ activity is controlled by multiple mechanisms, including the MST (and MAP4K)/LATS kinase cascade, RHO/ROCK signaling, and possibly FAK/SRC-catalyzed tyrosine phosphorylation of YAP (40,41). The interaction between these pathways remains unclear/controversial, but most of them regulate nuclear translocation of YAP/TAZ. MRTX-849 treatment also increased levels of nuclear YAP in H2030 cells, beginning at 4 hours and peaking at 24-48 hours (Fig. 3D). Similar results were obtained with other NSCLC lines (H2122, H23) and with the PDAC cell line MiaPaca2 (Fig. 3E**)**.

The delayed kinetics of YAP nuclear translocation following MRTX-849 treatment suggested a transcription-dependent process. As noted above, RHO/ROCK signaling can

promote YAP activation; also, *Rhoa* is required for mutant *Kras*-induced NSCLC in mice (42). Moreover, genes annotated as "Signaling by RHO GTPases", including several RHO family members (*RHOA*, *RHOB*, *RHOD*, Supplementary Table S3, Tabs 4-5, bold type), RHO-guanine nucleotide exchange factors (RHO-GEFs: *VAV2*, *TRIO*, *PICALM*, *ARGGEF10L*, *AKAP13*, Supplementary Table S3, Tabs 4-5, bold type), and possible RHO-GEFs (*ARHGEF40*, *PLEKHG4* Supplementary Table S3, Tab 4-5, bold type) were induced in both cell lines. RHO-mediated YAP activation is thought to be mediated via integrin activation, cytoskeletal reorganization, and actomyosin contractility (43,44). *FEMRT2*, encoding KINDLIN-2, which mediates integrin activation, was also induced in both lines (Supplementary Table S3, Tab 4-5, colored blue), as were *LIMK2*, which regulates COFILIN and promotes F-actin formation, *MYLK*, encoding myosin light chain kinase, a which regulates actomyosin contractility (Supplementary Table S3, Tab 4-5, colored orange) and multiple myosin genes (e.g., *MYL6, MYH9*, *MYH10*, *MYH14*, *MYL9*, *MYL12B*, *MYO6*, and others, Supplementary Table S3, Tab 4-5, colored red).

Collectively, these findings suggested that MRTX-849 treatment evokes a transcriptional program leading to increased integrin activation, cytoskeletal reorganization, actomyosin contractility, RHO activation and, consequently YAP/TAZ pathway activation. Consistent with this notion, RHO activity (assessed by G-LISA) increased following MRTX-849 treatment (Fig. 3F); genes annotated as "Signaling by RHO GTPases" were enriched in the SL screens (Fig. 1E), and the ROCK inhibitor Y27632 inhibited YAP nuclear translocation induced by MRTX-849 treatment for 24hr (Supplementary Fig. 3B) and to an even greater extent after 48h of treatment (Fig. 3G-H, quantified in Supplementary Fig. 3C-D). Y27632 addition also increased MRTX-849 efficacy in two cell lines tested (Fig. 3I and Supplementary Fig. 3E).

Mechanisms of Resistance to G12C/SHP2 Co-Inhibition in RAS-Driven NSCLC

We and others reported previously that SHP2 inhibition enhances G12Ci action *in vitro* and in mice (16,45,46), and multiple SHP2i are in clinical trials for $KRAS^{G12C}$-mutant tumors and other indications (e.g., NCT05480865, NCT03565003, NCT04916236, NCT04699188) (47). Anticipating that G12Ci/SHP2 combinations might show efficacy in patients, we performed CRISPR/Cas9 screens on combination-treated H2122, H2030, and H23 cells; HCC44 cells were too sensitive to the combination to obtain meaningful results. For these experiments, MRTX-849 was added at 2x IC50, and the clinical grade SHP2i TNO-155 was administered at its IC50 or 3 μM, its maximal dose (Supplementary Fig. 4A-B, Supplementary Table S4). For comparison, SL screens were carried out on the same lines treated with TNO-155, but will not be discussed here (Supplementary Table S5). Again, screen quality was high (Supplementary Fig. 4C), and multiple shared and unique SL "hits" were identified (Fig. 4A-C). Several genes were SL with single agent MRTX-849 and with MTRX-849/TNO-155 (indicated in red); others were unique to one treatment (Supplementary Fig. 4D). Likewise, shared SL pathways (PI3K/mTOR signaling, Glycolysis, N-linked glycosylation) were identified, but those (Signaling by ALK, Central Carbon Metabolism) unique to combination-treated cells also emerged (Fig. 4B and Supplementary Fig. 4D). Notably, *TEAD1* or *TEAD4* were hits in the MRTX849/TNO155

screen (Supplementary Fig. 4D), and genes annotated “Hippo signaling” were enriched as SL in the combination screen (Fig. 4B).

We therefore validated *TEAD1* and *TEAD4* as SL with MRTX-849/TNO155 using si- and shRNAs and dominant negative TEAD via studies analogous to those used for MRTX-849 alone (Fig. 4D-F). We also observed that combination therapy induced YAP nuclear translocation, consistent with a shared mechanism (Fig. 4G). These results suggest that TEAD inhibition could augment this drug combination as well as single agent MRTX-849.

TEAD Inhibitors Enhance The Efficacy of G12Ci in KRAS Mutant-Driven NSCLC

We next tested the effects of two mechanistically distinct TEAD inhibitors on MRTX-849 efficacy. MYF-03-69 is a tool compound that binds covalently to the conserved TEAD palmitate pocket, irreversibly disrupting YAP-TEAD association and suppressing TEAD1-4 transcriptional activity (48). VT-104 is a clinical grade, non-covalent, pan-TEAD inhibitor that also binds this pocket. Consistent with the above genetic results, both agents synergistically augmented MRTX-849 action in multiple NSCLC lines, including those that were not *STK11* and/or *KEAP1* mutant (Fig. 5A and B). This combination was also active in select PDAC and CRC cell lines (Fig. 5C and Fig. 5D). MYF-03-176 and VT-104 each showed higher IC50s (combined with MRTX-849 at its IC50 dose) in *YAP1* over-expressing KCL cells, arguing that their effects were on-target (Supplementary Fig. 5A and B). Furthermore, VT106, an inactive analog of VT-104 that does not block YAP/TEAD interaction (49), had no effect on drug sensitivity. VT-104 also increased the efficacy of combination MRTX849/TNO-155 in NSCLC lines (Supplementary Fig. 5C) compared with single agent therapy or two drug-combinations (all at reduced doses).

Given these pre-clinical data, we asked whether TEAD inhibition could enhance MRTX-849 efficacy in mice. At full doses (100 mg/kg/d), MRTX-849 is quite active against KCL syngeneic tumor grafts and H2030 cell-derived xenografts, resulting in complete responses (no detectable tumor) after 30 days of treatment. Some malignant cells remain, however, because after drug withdrawal, tumors recur. VT104 (10 mg/kg/d) has minimal single agent efficacy in either model. However, combining MRTX849 and VT104 results in a significant delay in tumor recurrence in both models (Fig. 5E and F). Collectively, then, combined G12C and TEAD inhibition shows increased efficacy over G12Ci alone *in vivo* as well as *in vitro*.

Resistance to G12Ci or G12Ci+SHP2i in Mouse and Human Induces Similar Pathways to Those Targeted by SL Genes

Next, we sought to further assess the relevance of our screen findings to the emergence of G12Ci resistance *in vivo*. To this end, we developed G12Ci- and G12Ci+SHP2i-resistant genetically engineered mouse models (GEMMs, see Methods for details). Briefly, LSL-$KRAS^{G12C}$;$Stk11^{fl/fl}$ (KCL) mice were infected with Ad-Cre to simultaneously activate the human *KRAS* transgene and delete *Stk11*. Mice were serially monitored by MRI. When tumors reached 300 mm^3 (2-3 months), long-term treatment with MRTX-849 (100 mg/kg, 5 days on/2 days off) was initiated and continued until tumors recurred (Fig. 6A). Three tumor-bearing mice were euthanized to obtain nodules, each of which was divided and

analyzed by RNA-seq and reverse phase protein array (RPPA). These results were compared with parental tumor samples, obtained from vehicle treated-mice.

RNA-seq revealed multiple enriched pathways ($p < 0.05$) that were also enriched in the CRISPR/Cas9 screens, including Fanconi anemia, MYC, E2F target, and glycosylation genes (Figure 6B, left panel, colored in red). Importantly, YAP/TAZ pathway signature genes (50) were markedly enriched in resistant nodules (Fig. 6B, right panel; Supplementary Fig. 6A, Supplementary Table S6). In line with these findings TAZ and TEAD were induced in RPPAs from MRTX-849-resistant tumors (Fig. 6C, full RPPA results are in Supplementary Table S7).

Other mice, whose tumors recurred after prolonged MRTX-849 treatment, were treated with MRTX849 (100mg/kg/d) plus the tool SHP2i SHP099 (75mg/kg/d). Addition of SHP099 resulted in partial responses, but tumors resistant to both agents (Combo-resistant tumors) soon recurred (Fig. 6A). RNA-seq of nodules from these tumors also revealed pathways common to the CRISPR/Cas9 SL genes (Fig. 6D, colored in red). For example, genes annotated as YAP and WWTR1-stimulated were induced, as were those associated with regulation of RHO activity and O-linked glycosylation (Fig. 6D; Supplementary Fig. 6B, Supplementary Table S8**)**. Other pathways were only associated with resistance to MRTX-849 (e.g., interferon signaling, VEGF signaling and others), or MRTX-849/SHP099-treatment (e.g., degradation of cytseine and homocysteine, PI3K events in ERBB2, PPAR signaling, and others) groups, respectively. Notably, TEAD and/or TAZ were also induced in RPPAs of nodules from MRTX-849/SHP099-treated mice (Fig. 6E, full results in Supplementary Table S9).

Finally, we analyzed sc-RNAseq data from tumor samples from two NSCLC patients with $KRAS^{G12C}$-mutant tumors: one developed resistance to sotorasib (AMG-510) and the other's tumor was resistant to MRTX-849 + TNO-155. We compared these data with scRNAseq of a $KRAS^{G12V}$-mutant NSCLC (Fig. 6F-G, Supplementary Table S10 and Supplementary Table S11). Remarkably, resistance pathways suggested by our CRISPR/Cas9 SL screens and the resistant GEMMs also were enriched in these patient samples. Importantly, Hippo and RHO GTPase signaling genes were enriched in both resistant tumors, along with glycolysis, MYC, glycosylation and mTOR signaling genes. Other pathways, including genes associated with epithelial-mesenchymal transition (EMT), Krebs cycle, DNA damage, KEAP1-NFE2L2 pathways, and autophagy, also were enriched in the human samples.

Validation of other shared SL genes from CRISPR/Cas9 screens

Finally, we tested the effect of knockdown of several other recurrent, potentially targetable SL genes. Reassuringly, siRNAs/shRNAs against *RIOK2* (Fig. 7A, Supplementary Fig. S7A) or *VRK1* (Fig. 7B, Supplementary Fig. S7B), which encode serine/threonine kinases, sensitized multiple NSCLC lines to MRTX-849 (at its IC50). VRK-IN-1(51), a tool VRK1 inhibitor, also enhanced G12Ci efficacy (Fig. 7C). Likewise, knockdown of *ELP3* and *ELP5* (Fig. 7D-E, Supplementary Fig. S7C-D), which encode components of the elongator complex (52), augmented MRTX-849 response. *ELP5* also scored as a significant SL gene in the MRTX-849 + TNO-155 screen (Fig. 4A), and *ELP5* siRNA enhanced the effect of

this combination (Fig. 7F). Similar results were obtained using doxycline-inducible shRNAs (Fig. 7G-I, Supplementary Fig. S7E-G). In concert, these data indicate that multiple other genes and pathways besides YAP/TAZ/TEAD could be targeted to enhance G12Ci efficacy.

DISCUSSION

The development of G12Cis was a major breakthrough in experimental therapeutics, yet their efficacy in the clinic has thus far been modest. The existence of multiple G12Ci resistance mechanisms indicates that combination therapies will be required to maximize the impact of these remarkable drugs. This need is particularly acute for the NSCLC subgroups with co-mutations in *STK11* and/or *KEAP1*, as well as for tumors of other histotypes (e.g., CRC) with $KRAS^{G12C}$ mutations. We identified recurrent synthetic lethal (SL) genes with G12Cis that span a range of functional classes, including genes in pathways related to Hippo and RHO signaling, tRNA processing, and heparan sulfate biosynthesis, as well as several novel kinases. Our results provide a landscape of potential new targets for future combination strategies, some of which can be tested rapidly in the clinic, others of which will require new drug development.

Two earlier studies used a similar CRISPR/Cas9 screening approch to search for G12Ci SL genes. Lou *et al.* (53) surveyed a NSCLC line, H358, and the PDAC line MIAPaCa-2, each maintained in 2D culture and treated with a tool G12Ci (ARS-1620). Han *et al.* studied H23 cells, which were also used here, maintained in 2D and 3D suspension (54). The “hits” in the earlier papers reveal some shared dependencies with our study (e.g., *ELP3*, *ELP4*, *PKN2*, *RPN1* in the H358 screen; *EXT1*, *WWTR1*, *SHOC2* in MIAPaCa-2 cells, *PGM3* in the 2D component of the 2D vs 3D screen; compare with Fig. 1D with References 43,44). Overall, however, the majority of our shared SL genes escaped detection in the prior studies, most likely because of differences in screening conditions, cell systems (including tumor histotype and co-mutations), the number of lines surveyed, and possibly the use of G12Cis at different stages of clinical development. In addition to expanding the landscape of G12Ci resistance genes and pathways, we also provide insight into resistance to G12Ci/SHP2i combination therapies.

Our G12Ci and G12Ci/SHP2i combination screens both identified the YAP/TAZ/TEAD pathway as a route to resistance *in vitro* and *in vivo*. We validated these findings genetically and pharmacologically using multiple cell lines, GEMM and CDX models, and two different modes of TEAD inhibition. Importantly, we also find evidence that this pathway is activated in mouse and human models of G12Ci and G12Ci +SHP2i-resistance. These findings comport with previous results implicating the YAP/TAZ/TEAD pathway in resistance to other targeted therapies (40,41) including MEKi and $BRAF^{V600E}$ inhibitors (36,55). Moreover, while our manuscript was in preparation, Hagenbeek *et al.* (56) reported the development of allosteric TEAD inhibitors and demonstrated their ability to block adaptive resistance to G12Ci treatment, while Adachi *et al.* (57) found similar effects of YAP1 deficiency in a limited number of NSCLC lines and H358 xenografts. Other TEAD inhibitors are already in phase 1 clinical trials (NCT05228015 and NCT04665206), and preliminary results indicate that at least one, VT3989, is safe with manageable toxicity (19).

We observed that YAP nuclear translocation and activity are induced by G12Ci treatment. At first glance, this finding was somewhat surprising, because previous work showed that LKB1 (encoded by *STK11*) antagonizes YAP activation by activating a PAR1->Scribble->MST2->LATs pathway; accordingly *STK11−/−* cells, as we screened here, should already have significant YAP activation (58). Indeed, consistent with the findings of Mohseni *et al.,* >50% of H2030 and 2122 cells show at least some nuclear localization of YAP (Fig. 3G-H, Supplementary Fig. S3C-D). This level of YAP activation could contribute to the relative refractoriness of *STK11−/−* NSCLC to multiple therapeutics (58) but it is clearly inadequate to confer complete G12Ci resistance *in vitro* or i*n vivo*. Multiple feedback pathways serve to limit YAP/TAZ/TEAD signaling (40) which dampen YAP activation in *STK11*-deficient cells and help explain this apparent paradox. Alternatively, or in addition, LKB1 activates DBL, a RHO-GEF(59). Hence, RHO levels are likely to be lower in *STK11−/−,* compared with *STK11*-replete cells, and thus inadequate to drive sufficient YAP translocation/activation to confer resistance.

Adachi *et al.* also observed G12Ci-induced YAP translocation in *STK11*-replete H358 cells and in LU65 cells, which are *STK11−/−*, but our studies differ in mechanistic detail. They reported that G12Ci treatment induces Scribble mislocalization, which leads to decreased MST2/LATS suppression of YAP nuclear localizaton. Although this model could be particularly relevant for *STK11*-replete cells, *STK11−/−* cells should already have mislocalized Scribble (58). By contrast, we find that MRTX-849 treatment induces the transcription of genes encoding multiple RHO paralogs and GEFs, as well as RHO targets, actin regulators, and myosins (including myosin-II). RHO, acting though the actomyosin cytoskeleton, is also known to promote YAP activation (40,41). Furthermore, earlier work found that RHOA is necessary for the transformation induced by mutant KRAS (60–62) and for $Kras^{G12D}$-driven lung adenocarcinoma (42), while suppressing ERK/MAPK signaling in cancer cells can result in increased RHOA activation (63). Consistent with our observations, inhibiting the RHO effector ROCK blocks MRTX-849-induced YAP nuclear translocation and adaptive resistance. The relationship between the MST2/LATS and RHO pathways for YAP activation remains controversial; specifically, it is unclear whether RHO acts via the MST2/YAP pathway or whether the latter is merely permissive for the former (40,41,44). Similarly, it is conceivable that Scribble mislocalization and RHO activation act in parallel in $KRAS^{G12C}$ NSCLC cells; in this regard, we note ROCK inhibitor treatment appeared to block YAP translocation only partially (Fig. 3G-H, Supplementary Fig. S3C-D). Alternatively, another RHO effector (e.g., mDIA, PKN) might play a role in YAP/TEAD pathway activation (Supplementary Fig. S3E). A possible role for PKN is particularly attractive, as it is also a SL target in our MTRX-849 screen.

Future studies are necessary to reveal how this RHO “regulome” is induced by G12Ci treatment, which RHO-GEFs are particularly important for increased RHO activity, and whether other RHO effectors are also important for YAP/TEAD pathway activation. Regardless, our finding that Y27632 enhances the effects of MRTX-849 raises the possibility that pharmacologically useful ROCK inhibitors, such as Fasudil, which is approved in Japan and China for the treatment of cerebral vasospasm (64), or others (65,66) might be repurposed for combining with G12Ci. ROCK inhibitors are not associated with proteinuria, and thus could avoid the major drug-related side effect of TEAD inhibition (65).

Adachi *et al*. also reported that, once activated, YAP drives increased expression of MRAS, which, by promoting assembly of the MRAS/SHOC2/PP1 complex, bypasses adaptive resistance to G12Ci. In agreement with their results, we also observed increases in MRAS RNA in adagrasib-treated H2030 and H2122 cells. Future studies should clarify the interplay between MRAS and RHO signaling in regulating Hippo signaling and adaptive resistance.

In addition to the RHO/YAP/TEAD pathway, we also validated two kinases (VRK1, RIOK2) and two tRNA-modifying enzymes (ELP3, ELP5) that scored as G12Ci SL genes. *VRK1* was previously reported as a "collateral lethality" in glioblastoma, owing to methylation and lack of expression of its paralog *VRK2* in this malignancy. *VRK1* depletion in these *VRK2*-deficient cells levels leads to a G2/M phase arrest, followed by DNA damage (67,68). By contrast, *VRK2* is expressed in NSCLC. We could not identify antibodies capable of detecting VRK2 by immunoblotting, but assuming that VRK2 is also expressed at the protein level, VRK1 must have specific functions in G12Ci-treated NSCLC cells. RIOK2 is a relatively unexplored RSK target whose normal function is to promote maturation of the 40S ribosome (69). ELP proteins comprise the so-called "elongator complex", which catalyzes tRNA modifications under various stresses. Previous research showed that suppression of *ELP1* or *ELP3* can abrogate vemurafenib in $BRAF^{V600E}$ melanoma (70), and that ELPs contribute to EGFR inhibitor resistance in breast cancer cells by promoting MCL1 synthesis (71). As the elongator complex has acetyl transferase activity, it might, like VRK1 and RIOK2, be amenable to future drug discovery efforts. Furthermore, *VRK1*, *ELP3*, and *ELP5* expression were significantly increased in the AMG-510-resistant patient sample, while *RIOK2* levels were nominally increased (Supplementary Table S10).

In addition to the SL genes that we validated, our screens have identified other potentially targetable gens and pathways. For example, several genes encoding glycolytic enzymes were hits in our screens. Several of these genes also showed increased expression infollowing adagrasib treatment of lung cancer cell lines (Fig. 1E, 3C, 4B, and Supplementary Table 3). , and glycolytic pathway genes were also induced in our G12Ci-resistant samples (Fig. 6G). Mutant KRAS is a well known regulator of glycolysis (72), and STK11 is also a critical regulator of metabolism via its substrate AMPK (73). Furthermore, previous studies have revealed complex, bidirectional interplay between the Hippo pathway and glucose metabolism (74). Additionally, the synthetic lethality with DNA damage genes (Fanconi anemia pathway, Fig. 1E) suggests the potential for synergy between G12Cis and some conventional chemotherapy agents. Several of these genes also showed increased expression in G12Ci-resistant samples (6B, 6F-G). Future work will explore the relationship between these and the other SL pathways identified herein and their utility in combination therapy with G12Cis.

Supplementary Material

Refer to Web version on PubMed Central for supplementary material.

ACKNOWLEDGMENTS

We thank the PCC Genome Technology Center (GTC) shared resource for expert library preparation and sequencing, NYU Langone Preclinical Imaging Laboratory (PIL) for MRI;and the Applied Bioinformatics

Laboratories (ABL) shared resources for bioinformatics support and help with data analysis and interpretation. GTC, ABL are supported by P30CA016087 and PIL is supported by NIH/NCI 5P30CA016087 and NIH P41 EB017183. We thank Drs. Leonard Post, Gordon B. Mills, John T. Poirier, Diane M. Simeone, Jiehui Deng, Ting Chen, Han Han, and all other Neel lab and Wong lab members for helpful advice and discussions. This work was supported by NIH grant CA248896 (to B.G. Neel and K.-K. Wong).

CONFLICT OF INTEREST:

B.G.N. is a founder of, holds equity in, and receives consulting fees from Lighthorse Therapeutics and Aethon Therapeutics, and is a founder of, and holds equity in, Northern Biologics, LP and Navire Pharma. He also receives consulting fees and equity from Arvinas, Inc., and holds equity in Recursion Pharma. He has sponsored research agreements with Mirati and Repare Therapeutics. His spouse owns equity in Moderna, Inc. and Revolution Medicines, Inc., and during the course of these experiments also had equity in Mirati Therapeutics. **K.-K.W**. is a founder and equity holder of G1 Therapeutics and has sponsored research agreements with Takeda, TargImmune, Bristol-Myers Squibb (BMS), Mirati, Merus, Revolution Medicine and Alkermes and consulting and sponsored research agreements with AstraZeneca, Janssen, Pfizer, Novartis, Merck, Zentalis, BridgeBio, and Blueprint, as well as consulting agreements and equity with Recursion, Cogent and Allorion. **J.G.C.** is a Mirati employee, fiduciary officer, and shareholder. **V.V.** is a consultant/advisory role in BMS, Merck, AstraZeneca, Amgen, Janssen Oncology, and Picture Health. **T.T. T.** reports employment with Vivace Therapeutics and has an equity interest in Vivace Therapeutics. **T.Z**. is a scientific founder, equity holder, and consultant of Matchpoint, equity holder of Shenandoah, and consultant of Lighthorse. **N.S.G.** is a founder, science advisory board member (SAB) and equity holder in Syros, C4, Allorion, Lighthorse, Voronoi, Inception, Matchpoint, CobroVentures, GSK, Shenandoah (board member), Larkspur (board member) and Soltego (board member). **B.G.N, K.-K.W.** and **S.M.** have submitted a provisional patent application related to this work.

REFERENCES:

1. Yaeger R, Chatila WK, Lipsyc MD, Hechtman JF, Cercek A, Sanchez-Vega F, et al. Clinical Sequencing Defines the Genomic Landscape of Metastatic Colorectal Cancer. Cancer Cell 2018;33:125–36 e3 [PubMed: 29316426]
2. Campbell JD, Alexandrov A, Kim J, Wala J, Berger AH, Pedamallu CS, et al. Distinct patterns of somatic genome alterations in lung adenocarcinomas and squamous cell carcinomas. Nat Genet 2016;48:607–16 [PubMed: 27158780]
3. Bailey P, Chang DK, Nones K, Johns AL, Patch AM, Gingras MC, et al. Genomic analyses identify molecular subtypes of pancreatic cancer. Nature 2016;531:47–52 [PubMed: 26909576]
4. Arbour KC, Jordan E, Kim HR, Dienstag J, Yu HA, Sanchez-Vega F, et al. Effects of Co-occurring Genomic Alterations on Outcomes in Patients with KRAS-Mutant Non-Small Cell Lung Cancer. Clin Cancer Res 2018;24:334–40 [PubMed: 29089357]
5. Skoulidis F, Byers LA, Diao L, Papadimitrakopoulou VA, Tong P, Izzo J, et al. Co-occurring genomic alterations define major subsets of KRAS-mutant lung adenocarcinoma with distinct biology, immune profiles, and therapeutic vulnerabilities. Cancer Discov 2015;5:860–77 [PubMed: 26069186]
6. Negrao MV, Araujo HA, Lamberti G, Cooper AJ, Akhave NS, Zhou T, et al. Co-mutations and KRAS G12C inhibitor efficacy in advanced NSCLC. Cancer Discov 2023
7. Papillon-Cavanagh S, Doshi P, Dobrin R, Szustakowski J, Walsh AM. STK11 and KEAP1 mutations as prognostic biomarkers in an observational real-world lung adenocarcinoma cohort. ESMO Open 2020;5
8. Punekar SR, Velcheti V, Neel BG, Wong KK. The current state of the art and future trends in RAS-targeted cancer therapies. Nat Rev Clin Oncol 2022;19:637–55 [PubMed: 36028717]
9. Dy GK, Govindan R, Velcheti V, Falchook GS, Italiano A, Wolf J, et al. Long-Term Outcomes and Molecular Correlates of Sotorasib Efficacy in Patients With Pretreated KRAS G12C-Mutated Non-Small-Cell Lung Cancer: 2-Year Analysis of CodeBreaK 100. J Clin Oncol 2023;41:3311–7 [PubMed: 37098232]
10. Janne PA, Riely GJ, Gadgeel SM, Heist RS, Ou SI, Pacheco JM, et al. Adagrasib in Non-Small-Cell Lung Cancer Harboring a KRAS(G12C) Mutation. N Engl J Med 2022;387:120–31 [PubMed: 35658005]

11. Falchook G, Li BT, Marrone KA, Bestvina CM, Langer CJ, Krauss JC, et al. OA03.03 Sotorasib in Combination with RMC-4630, a SHP2 Inhibitor, in KRAS p.G12C-Mutated NSCLC and Other Solid Tumors. Journal of Thoracic Oncology 2022;17:S8
12. Skoulidis F, Li BT, Dy GK, Price TJ, Falchook GS, Wolf J, et al. Sotorasib for Lung Cancers with KRAS p.G12C Mutation. N Engl J Med 2021;384:2371–81 [PubMed: 34096690]
13. de Langen AJ, Johnson ML, Mazieres J, Dingemans AC, Mountzios G, Pless M, et al. Sotorasib versus docetaxel for previously treated non-small-cell lung cancer with KRAS(G12C) mutation: a randomised, open-label, phase 3 trial. Lancet 2023;401:733–46 [PubMed: 36764316]
14. Weiss A, Lorthiois E, Barys L, Beyer KS, Bomio-Confaglia C, Burks H, et al. Discovery, Preclinical Characterization, and Early Clinical Activity of JDQ443, a Structurally Novel, Potent, and Selective Covalent Oral Inhibitor of KRASG12C. Cancer Discov 2022;12:1500–17 [PubMed: 35404998]
15. Ryan MB, Coker O, Sorokin A, Fella K, Barnes H, Wong E, et al. KRAS(G12C)-independent feedback activation of wild-type RAS constrains KRAS(G12C) inhibitor efficacy. Cell Rep 2022;39:110993 [PubMed: 35732135]
16. Fedele C, Li S, Teng KW, Foster CJR, Peng D, Ran H, et al. SHP2 inhibition diminishes KRASG12C cycling and promotes tumor microenvironment remodeling. J Exp Med 2021;218
17. Pan Y, Han H, Hu H, Wang H, Song Y, Hao Y, et al. KMT2D deficiency drives lung squamous cell carcinoma and hypersensitivity to RTK-RAS inhibition. Cancer Cell 2023;41:88–105 e8 [PubMed: 36525973]
18. Hart T, Tong AHY, Chan K, Van Leeuwen J, Seetharaman A, Aregger M, et al. Evaluation and Design of Genome-Wide CRISPR/SpCas9 Knockout Screens. G3 (Bethesda) 2017;7:2719–27 [PubMed: 28655737]
19. Olivieri M, Durocher D. Genome-scale chemogenomic CRISPR screens in human cells using the TKOv3 library. STAR Protoc 2021;2:100321 [PubMed: 33598657]
20. Li W, Xu H, Xiao T, Cong L, Love MI, Zhang F, et al. MAGeCK enables robust identification of essential genes from genome-scale CRISPR/Cas9 knockout screens. Genome Biol 2014;15:554 [PubMed: 25476604]
21. Kuleshov MV, Jones MR, Rouillard AD, Fernandez NF, Duan Q, Wang Z, et al. Enrichr: a comprehensive gene set enrichment analysis web server 2016 update. Nucleic Acids Res 2016;44:W90–7 [PubMed: 27141961]
22. Subramanian A, Tamayo P, Mootha VK, Mukherjee S, Ebert BL, Gillette MA, et al. Gene set enrichment analysis: a knowledge-based approach for interpreting genome-wide expression profiles. Proc Natl Acad Sci U S A 2005;102:15545–50 [PubMed: 16199517]
23. Zhou Y, Zhou B, Pache L, Chang M, Khodabakhshi AH, Tanaseichuk O, et al. Metascape provides a biologist-oriented resource for the analysis of systems-level datasets. Nat Commun 2019;10:1523 [PubMed: 30944313]
24. Zhao W, Sachsenmeier K, Zhang L, Sult E, Hollingsworth RE, Yang H. A New Bliss Independence Model to Analyze Drug Combination Data. J Biomol Screen 2014;19:817–21 [PubMed: 24492921]
25. Liao Y, Smyth GK, Shi W. featureCounts: an efficient general purpose program for assigning sequence reads to genomic features. Bioinformatics 2014;30:923–30 [PubMed: 24227677]
26. Akbani R, Ng PK, Werner HM, Shahmoradgoli M, Zhang F, Ju Z, et al. A pan-cancer proteomic perspective on The Cancer Genome Atlas. Nat Commun 2014;5:3887 [PubMed: 24871328]
27. Ji H, Ramsey MR, Hayes DN, Fan C, McNamara K, Kozlowski P, et al. LKB1 modulates lung cancer differentiation and metastasis. Nature 2007;448:807–10 [PubMed: 17676035]
28. Li S, Liu S, Deng J, Akbay EA, Hai J, Ambrogio C, et al. Assessing Therapeutic Efficacy of MEK Inhibition in a KRAS(G12C)-Driven Mouse Model of Lung Cancer. Clin Cancer Res 2018;24:4854–64 [PubMed: 29945997]
29. Skoulidis F, Arbour KC, Hellmann MD, Patil PD, Marmarelis ME, Awad MM, et al. Association of STK11/LKB1 genomic alterations with lack of benefit from the addition of pembrolizumab to platinum doublet chemotherapy in non-squamous non-small cell lung cancer. Journal of Clinical Oncology 2019;37:102-

30. West HJ, McCleland M, Cappuzzo F, Reck M, Mok TS, Jotte RM, et al. Clinical efficacy of atezolizumab plus bevacizumab and chemotherapy in KRAS-mutated non-small cell lung cancer with STK11, KEAP1, or TP53 comutations: subgroup results from the phase III IMpower150 trial. Journal for Immunotherapy of Cancer 2022;10
31. Mair B, Tomic J, Masud SN, Tonge P, Weiss A, Usaj M, et al. Essential Gene Profiles for Human Pluripotent Stem Cells Identify Uncharacterized Genes and Substrate Dependencies. Cell Rep 2019;27:599–615 e12 [PubMed: 30970261]
32. Sulahian R, Kwon JJ, Walsh KH, Pailler E, Bosse TL, Thaker M, et al. Synthetic Lethal Interaction of SHOC2 Depletion with MEK Inhibition in RAS-Driven Cancers. Cell Rep 2019;29:118–34 e8 [PubMed: 31577942]
33. Kim D, Xue JY, Lito P. Targeting KRAS(G12C): From Inhibitory Mechanism to Modulation of Antitumor Effects in Patients. Cell 2020;183:850–9 [PubMed: 33065029]
34. Brooks AN, Kilgour E, Smith PD. Molecular pathways: fibroblast growth factor signaling: a new therapeutic opportunity in cancer. Clin Cancer Res 2012;18:1855–62 [PubMed: 22388515]
35. Pobbati AV, Kumar R, Rubin BP, Hong W. Therapeutic targeting of TEAD transcription factors in cancer. Trends Biochem Sci 2023;48:450–62 [PubMed: 36709077]
36. Nguyen CDK, Yi C. YAP/TAZ Signaling and Resistance to Cancer Therapy. Trends Cancer 2019;5:283–96 [PubMed: 31174841]
37. Yuan Y, Park J, Feng A, Awasthi P, Wang Z, Chen Q, et al. YAP1/TAZ-TEAD transcriptional networks maintain skin homeostasis by regulating cell proliferation and limiting KLF4 activity. Nat Commun 2020;11:1472 [PubMed: 32193376]
38. Rosenbluh J, Nijhawan D, Cox AG, Li X, Neal JT, Schafer EJ, et al. beta-Catenin-driven cancers require a YAP1 transcriptional complex for survival and tumorigenesis. Cell 2012;151:1457–73 [PubMed: 23245941]
39. Zhao B, Ye X, Yu J, Li L, Li W, Li S, et al. TEAD mediates YAP-dependent gene induction and growth control. Genes Dev 2008;22:1962–71 [PubMed: 18579750]
40. Franklin JM, Wu Z, Guan KL. Insights into recent findings and clinical application of YAP and TAZ in cancer. Nat Rev Cancer 2023
41. Piccolo S, Panciera T, Contessotto P, Cordenonsi M. YAP/TAZ as master regulators in cancer: modulation, function and therapeutic approaches. Nat Cancer 2023;4:9–26 [PubMed: 36564601]
42. Konstantinidou G, Ramadori G, Torti F, Kangasniemi K, Ramirez RE, Cai Y, et al. RHOA-FAK is a required signaling axis for the maintenance of KRAS-driven lung adenocarcinomas. Cancer Discov 2013;3:444–57 [PubMed: 23358651]
43. Yu FX, Zhao B, Guan KL. Hippo Pathway in Organ Size Control, Tissue Homeostasis, and Cancer. Cell 2015;163:811–28 [PubMed: 26544935]
44. Totaro A, Panciera T, Piccolo S. YAP/TAZ upstream signals and downstream responses. Nat Cell Biol 2018;20:888–99 [PubMed: 30050119]
45. Ryan MB, Fece de la Cruz F, Phat S, Myers DT, Wong E, Shahzade HA, et al. Vertical Pathway Inhibition Overcomes Adaptive Feedback Resistance to KRAS(G12C) Inhibition. Clin Cancer Res 2020;26:1633–43 [PubMed: 31776128]
46. Ahmed TA, Adamopoulos C, Karoulia Z, Wu X, Sachidanandam R, Aaronson SA, et al. SHP2 Drives Adaptive Resistance to ERK Signaling Inhibition in Molecularly Defined Subsets of ERK-Dependent Tumors. Cell Rep 2019;26:65–78 e5 [PubMed: 30605687]
47. Kerr DL, Haderk F, Bivona TG. Allosteric SHP2 inhibitors in cancer: Targeting the intersection of RAS, resistance, and the immune microenvironment. Curr Opin Chem Biol 2021;62:1–12 [PubMed: 33418513]
48. Fan M, Lu W, Che J, Kwiatkowski NP, Gao Y, Seo HS, et al. Covalent disruptor of YAP-TEAD association suppresses defective Hippo signaling. Elife 2022;11
49. Tang TT, Konradi AW, Feng Y, Peng X, Ma M, Li J, et al. Small Molecule Inhibitors of TEAD Auto-palmitoylation Selectively Inhibit Proliferation and Tumor Growth of NF2-deficient Mesothelioma. Mol Cancer Ther 2021;20:986–98 [PubMed: 33850002]
50. Cordenonsi M, Zanconato F, Azzolin L, Forcato M, Rosato A, Frasson C, et al. The Hippo transducer TAZ confers cancer stem cell-related traits on breast cancer cells. Cell 2011;147:759–72 [PubMed: 22078877]

51. Serafim RAM, de Souza Gama FH, Dutra LA, Dos Reis CV, Vasconcelos SNS, da Silva Santiago A, et al. Development of Pyridine-based Inhibitors for the Human Vaccinia-related Kinases 1 and 2. ACS Med Chem Lett 2019;10:1266–71 [PubMed: 31531195]
52. Gaik M, Kojic M, Wainwright BJ, Glatt S. Elongator and the role of its subcomplexes in human diseases. EMBO Mol Med 2023;15:e16418 [PubMed: 36448458]
53. Lou K, Steri V, Ge AY, Hwang YC, Yogodzinski CH, Shkedi AR, et al. KRAS(G12C) inhibition produces a driver-limited state revealing collateral dependencies. Sci Signal 2019;12
54. Han K, Pierce SE, Li A, Spees K, Anderson GR, Seoane JA, et al. CRISPR screens in cancer spheroids identify 3D growth-specific vulnerabilities. Nature 2020;580:136–41 [PubMed: 32238925]
55. Dey A, Varelas X, Guan KL. Targeting the Hippo pathway in cancer, fibrosis, wound healing and regenerative medicine. Nat Rev Drug Discov 2020;19:480–94 [PubMed: 32555376]
56. Hagenbeek TJ, Zbieg JR, Hafner M, Mroue R, Lacap JA, Sodir NM, et al. An allosteric pan-TEAD inhibitor blocks oncogenic YAP/TAZ signaling and overcomes KRAS G12C inhibitor resistance. Nat Cancer 2023;4:812–28 [PubMed: 37277530]
57. Adachi Y, Kimura R, Hirade K, Yanase S, Nishioka Y, Kasuga N, et al. Scribble mis-localization induces adaptive resistance to KRAS G12C inhibitors through feedback activation of MAPK signaling mediated by YAP-induced MRAS. Nat Cancer 2023;4:829–43 [PubMed: 37277529]
58. Mohseni M, Sun J, Lau A, Curtis S, Goldsmith J, Fox VL, et al. A genetic screen identifies an LKB1-MARK signalling axis controlling the Hippo-YAP pathway. Nat Cell Biol 2014;16:108–17 [PubMed: 24362629]
59. Xu X, Omelchenko T, Hall A. LKB1 tumor suppressor protein regulates actin filament assembly through Rho and its exchange factor Dbl independently of kinase activity. BMC Cell Biol 2010;11:77 [PubMed: 20939895]
60. Khosravi-Far R, Solski PA, Clark GJ, Kinch MS, Der CJ. Activation of Rac1, RhoA, and mitogen-activated protein kinases is required for Ras transformation. Mol Cell Biol 1995;15:6443–53 [PubMed: 7565796]
61. Chen JC, Zhuang S, Nguyen TH, Boss GR, Pilz RB. Oncogenic Ras leads to Rho activation by activating the mitogen-activated protein kinase pathway and decreasing Rho-GTPase-activating protein activity. J Biol Chem 2003;278:2807–18 [PubMed: 12429740]
62. Qiu RG, Chen J, McCormick F, Symons M. A role for Rho in Ras transformation. Proc Natl Acad Sci U S A 1995;92:11781–5 [PubMed: 8524848]
63. Vial E, Sahai E, Marshall CJ. ERK-MAPK signaling coordinately regulates activity of Rac1 and RhoA for tumor cell motility. Cancer Cell 2003;4:67–79 [PubMed: 12892714]
64. Zhao J, Zhou D, Guo J, Ren Z, Zhou L, Wang S, et al. Effect of fasudil hydrochloride, a protein kinase inhibitor, on cerebral vasospasm and delayed cerebral ischemic symptoms after aneurysmal subarachnoid hemorrhage. Neurol Med Chir (Tokyo) 2006;46:421–8 [PubMed: 16998274]
65. Barcelo J, Samain R, Sanz-Moreno V. Preclinical to clinical utility of ROCK inhibitors in cancer. Trends Cancer 2023;9:250–63 [PubMed: 36599733]
66. Kim S, Kim SA, Han J, Kim IS. Rho-Kinase as a Target for Cancer Therapy and Its Immunotherapeutic Potential. Int J Mol Sci 2021;22
67. Shields JA, Meier SR, Bandi M, Mulkearns-Hubert EE, Hajdari N, Ferdinez MD, et al. VRK1 Is a Synthetic-Lethal Target in VRK2-Deficient Glioblastoma. Cancer Res 2022;82:4044–57 [PubMed: 36069976]
68. So J, Mabe NW, Englinger B, Chow KH, Moyer SM, Yerrum S, et al. VRK1 as a synthetic lethal target in VRK2 promoter-methylated cancers of the nervous system. JCI Insight 2022;7
69. Cerezo EL, Houles T, Lie O, Sarthou MK, Audoynaud C, Lavoie G, et al. RIOK2 phosphorylation by RSK promotes synthesis of the human small ribosomal subunit. PLoS Genet 2021;17:e1009583 [PubMed: 34125833]
70. Rapino F, Delaunay S, Rambow F, Zhou Z, Tharun L, De Tullio P, et al. Codon-specific translation reprogramming promotes resistance to targeted therapy. Nature 2018;558:605–9 [PubMed: 29925953]

71. Cruz-Gordillo P, Honeywell ME, Harper NW, Leete T, Lee MJ. ELP-dependent expression of MCL1 promotes resistance to EGFR inhibition in triple-negative breast cancer cells. Sci Signal 2020;13

72. Mukhopadhyay S, Vander Heiden MG, McCormick F. The Metabolic Landscape of RAS-Driven Cancers from biology to therapy. Nat Cancer 2021;2:271–83 [PubMed: 33870211]

73. Shackelford DB, Shaw RJ. The LKB1-AMPK pathway: metabolism and growth control in tumour suppression. Nat Rev Cancer 2009;9:563–75 [PubMed: 19629071]

74. Koo JH, Guan KL. Interplay between YAP/TAZ and Metabolism. Cell Metab 2018;28:196–206 [PubMed: 30089241]

STATEMENT OF SIGNIFICANCE

Identification of synthetic lethal genes with $KRAS^{G12C}$ inhibitors using genome-wide CRISPR/Cas9 screening and credentialing of the ability of TEAD inhibition to enhance $KRAS^{G12C}$ inhibitor efficacy provides a roadmap for combination strategies.

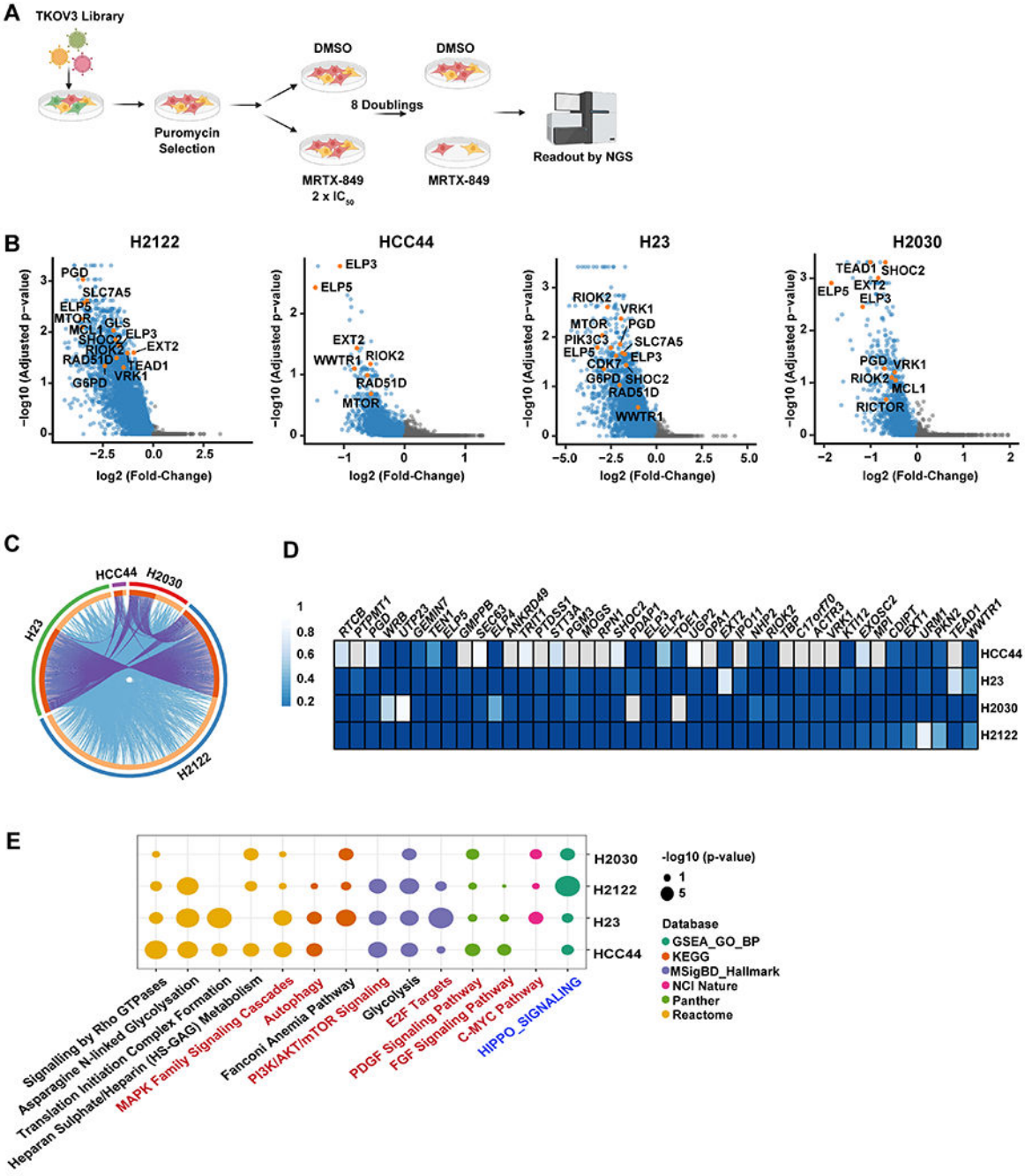

Figure 1. Genome-wide CRISPR/Cas9 screens identify MRTX-849 synthetic lethal (SL) genes.

A, Schematic showing CRISPR/Cas9 screening strategy **B,** Volcano plots showing results of genome-wide CRISPR/Cas9 screens of *KRAS*^{G12C};*STK11* co-mutated non-small cell lung cancer (NSCLC) cell lines, analyzed by MaGeCK; orange circles indicate select SL genes (FDR <0.1) **C,** Circos plot showing overlap of SL genes in NSCLC lines (FDR<0.1). Outside arcs show SL genes within each line. Inside arcs show SL genes shared in multiple lines (dark orange) and those unique to individual lines (light orange). Purple lines show which cells share a given SL gene. The greater the number of purple links and the size of

the dark orange arcs, the greater the overlap of SL genes between cell lines. **D,** Heat map showing select SL genes across the four cell lines. Color code indicates FDR for each gene in each line (scale at left). **E,** Bubble plot indicates enriched pathways ($p < 0.05$) of SL genes (FDR < 0.1). Datasets used for pathway analysis are color-coded as shown on right side. Size of circle indicates significance of each pathway assignment.

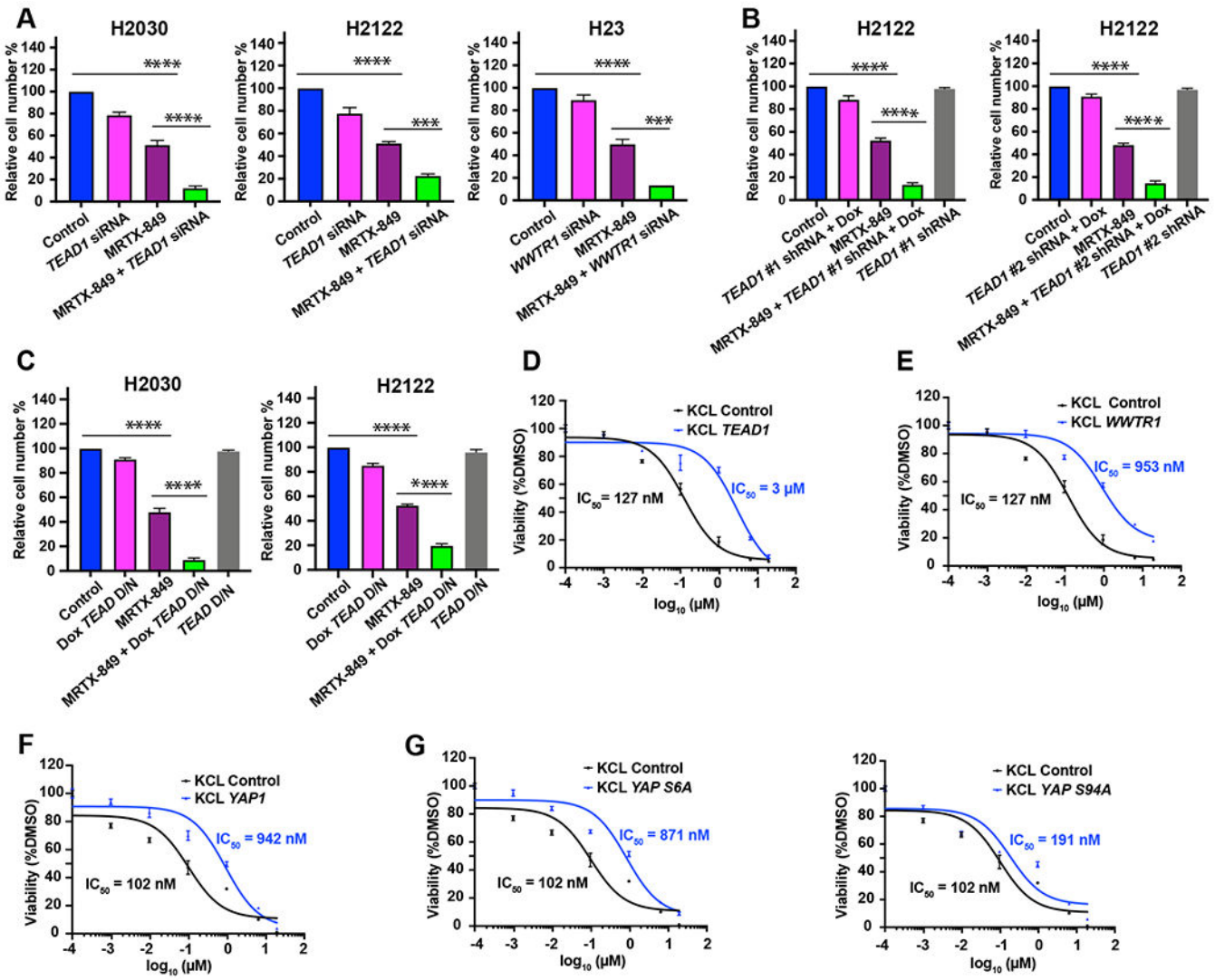

Figure 2. Validation of YAP/TAZ/TEAD pathway genes.

A, Trypan blue-based proliferation assays (5 days) on indicated cell lines treated with *TEAD1* or *WWTR1* siRNA, as indicated, and/or MRTX-849 (at IC50), normalized to untreated (Control) cells, ****p<0.0001, *** p<0.001, 1-way ANOVA with Tukey's multiple comparisons test. **B,** Proliferation assays on H2122 cells stably transduced with lentiviruses expressing either of two doxycycline-inducible *TEAD1* shRNAs or control shRNA and treated with MRTX-849 (at IC50) of vehicle with or without prior doxycycline (Dox) treatment for 96 hr, ****p<0.0001, 1-way ANOVA with Tukey's multiple comparisons test **C,** Proliferation assays on 72 hr Dox-induced H2030 and H2122 cell lines transduced with doxycycline-inducible dominant negative *TEAD* and treated with MRTX-849 (at IC50) or vehicle, as indicated, ****p<0.0001, 1-way ANOVA with Tukey's multiple comparisons test. **D-F,** MRTX-849 dose-response curves (using modified MTS assay) for the indicated mouse cell lines stably overexpressing *TEAD1*(**D**), *WWTR1* (**E**), *YAP1* (**F**) or *YAP1* mutants (**G**). IC50s were determined by GraphPad Prism.

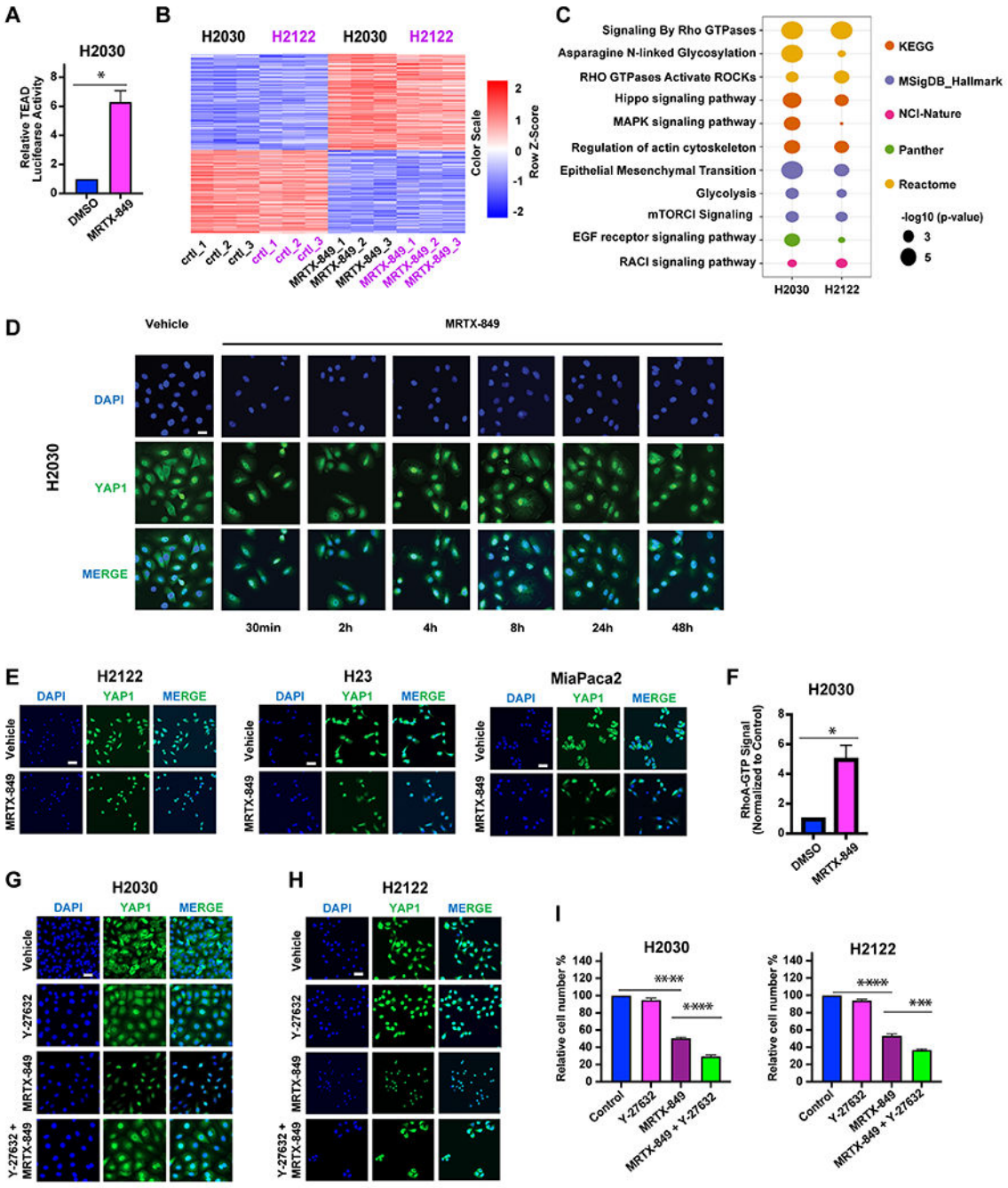

Figure 3. MRTX-849 treatment induces RHO/ROCK-dependent nuclear translocation of YAP.

A, H2030 cells were treated with MRTX-849 (at IC50) for 48 hrs, and the activity of the TEAD-responsive 8XGIITC-Luc reporter, normalized to a co-transfected Renilla luciferase construct, was determined. *p<0.05, Student's *t*-test **B,** Heat map showing results of bulk RNA-seq of H2030 and H2122 cells treated with MRTX-849 (at IC50) for 48 hr in triplicate **C,** Bubble plot indicates pathways enriched ($p < 0.05$) in up-regulated genes (FDR < 0.1). Datasets (color-coded) used for pathway analysis are indicated at right with size of circles indicating significance. **D,** Immunofluorescence images showing YAP1 and DAPI staining

of representative fields of H2030 cells treated with MRTX-849 (at IC50) for the indicated times. **E,** YAP1 and DAPI immunofluorescence of H2122, H23, and MiaPaca2 cells treated with MRTX-849 (at their respective IC50s) for 48 hrs. **F,** MRTX-849 treatment causes increased RHOA activity. H2030 cells were treated with MRTX-849 (at IC50) for 48h, and RHOA-GTP was quantified by ELISA. Luminescence at A490nm in treated samples normalized to DMSO-treated values is shown. *p<0.05, Student's *t*-test **G-H,** ROCK inhibitor treatment impairs MRTX-849-induced YAP1 nuclear localization. The indicated NSCLC lines were treated with MRTX-849 (at IC50) with or without the ROCK inhibitor Y-27632 (10 μM), and YAP1 localization was assessed by immunofluorescence (with DAPI staining to identify nuclei). **I,** Trypan blue-based proliferation assays on H2030 and H2122 cell lines treated with MRTX-849 (at IC50) alone or with Y-27632 (10 μM) as indicated, normalized to untreated (Control) cells. ****p<0.0001, ***p<0.001, 1-way ANOVA with Tukey's multiple comparisons test. All immunofluorescence images are representative of three independent experiments. Scale bar=20 μm

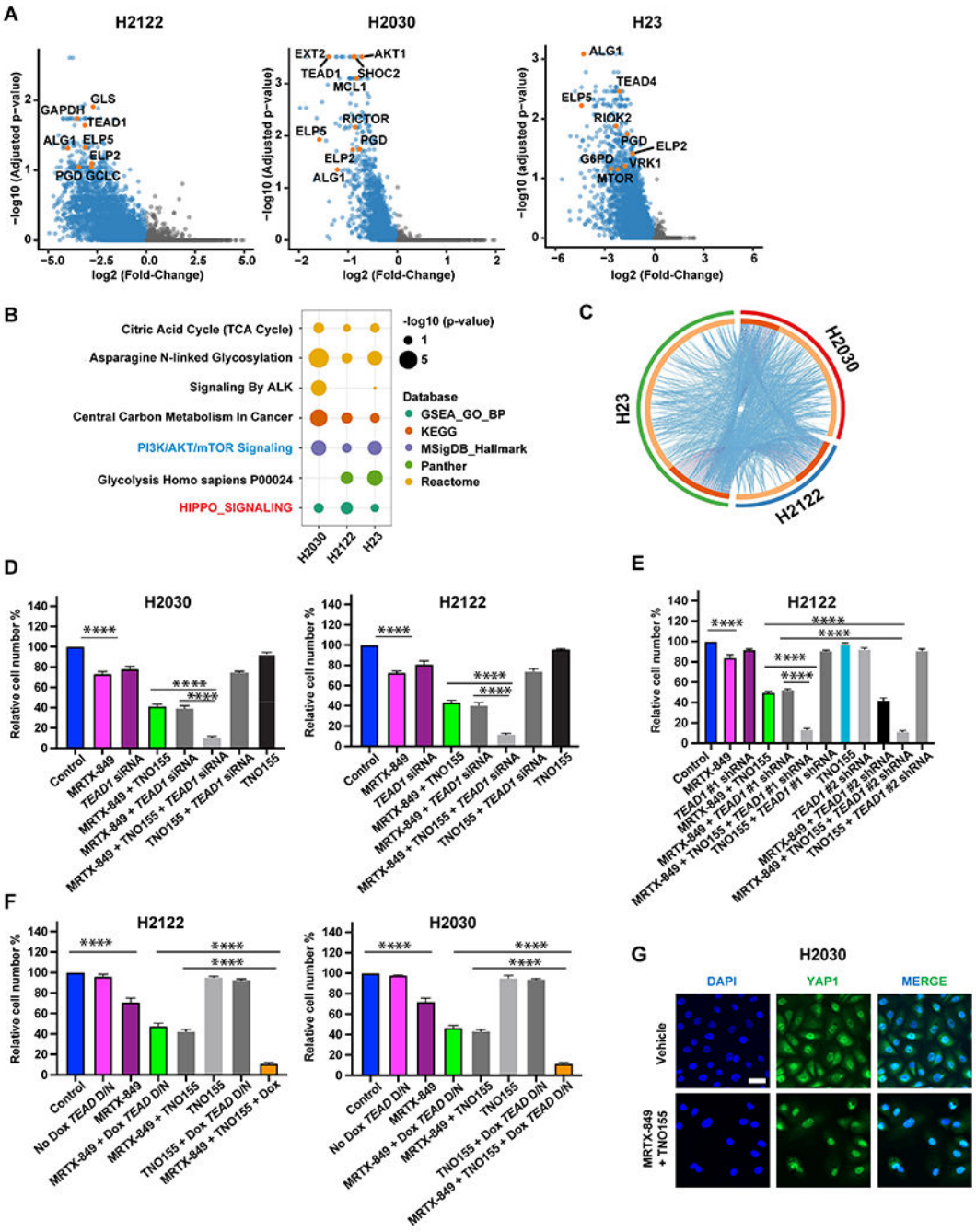

Figure 4. Whole-genome CRISPR screens for MRTX-849 + TNO155 synthetic lethal genes.

A, Genome-wide CRISPR/Cas9 SL screens of H2122, H23, and H2030 cells in the presence or absence of MRTX-849 + TNO155 (at doses described in Results) were analyzed using MaGeCK. Select SL genes (FDR<0.1) are indicated by orange circles. **B,** Bubble plot shows pathways (p<0.05) enriched in SL genes (FDR< 0.1). Datasets used for analysis are color-coded at right; size of circle indicates significance level. **C,** Circos plot illustrating overlap of SL genes (FDR<0.1) between lines. **D,** Trypan-blue-based proliferation assays on H2030 and H2122 cell lines transfected with *TEAD1* siRNA (where indicated) or

scrambled control siRNA and treated with vehicle or MRTX-849 and/or TNO155 (at half the IC25 for both drugs) , as indicated. . ****p<0.0001, 1-way ANOVA and Tukey's multiple comparisons test **E,** Proliferation of H2122 cells expressing two different *TEAD1* shRNA and treated with MRTX-849 and/or TNO155, as indicated (IC25 dosage for both of the drugs). ****p<0.0001, 1-way ANOVA and Tukey's multiple comparisons test **F,** Effects of dominant negative TEAD and MRTX-849 and/or TNO155 (IC25 dose) on proliferation of H2030 and H2122 cells. ****p<0.0001, 1-way ANOVA and Tukey's multiple comparisons test. **G,** Representative YAP1 and DAPI immunofluorescence images (from 3 independent experiments) of H2030 cells treated with MRTX-849+TNO155 (each at respective IC0) for 48 hrs.

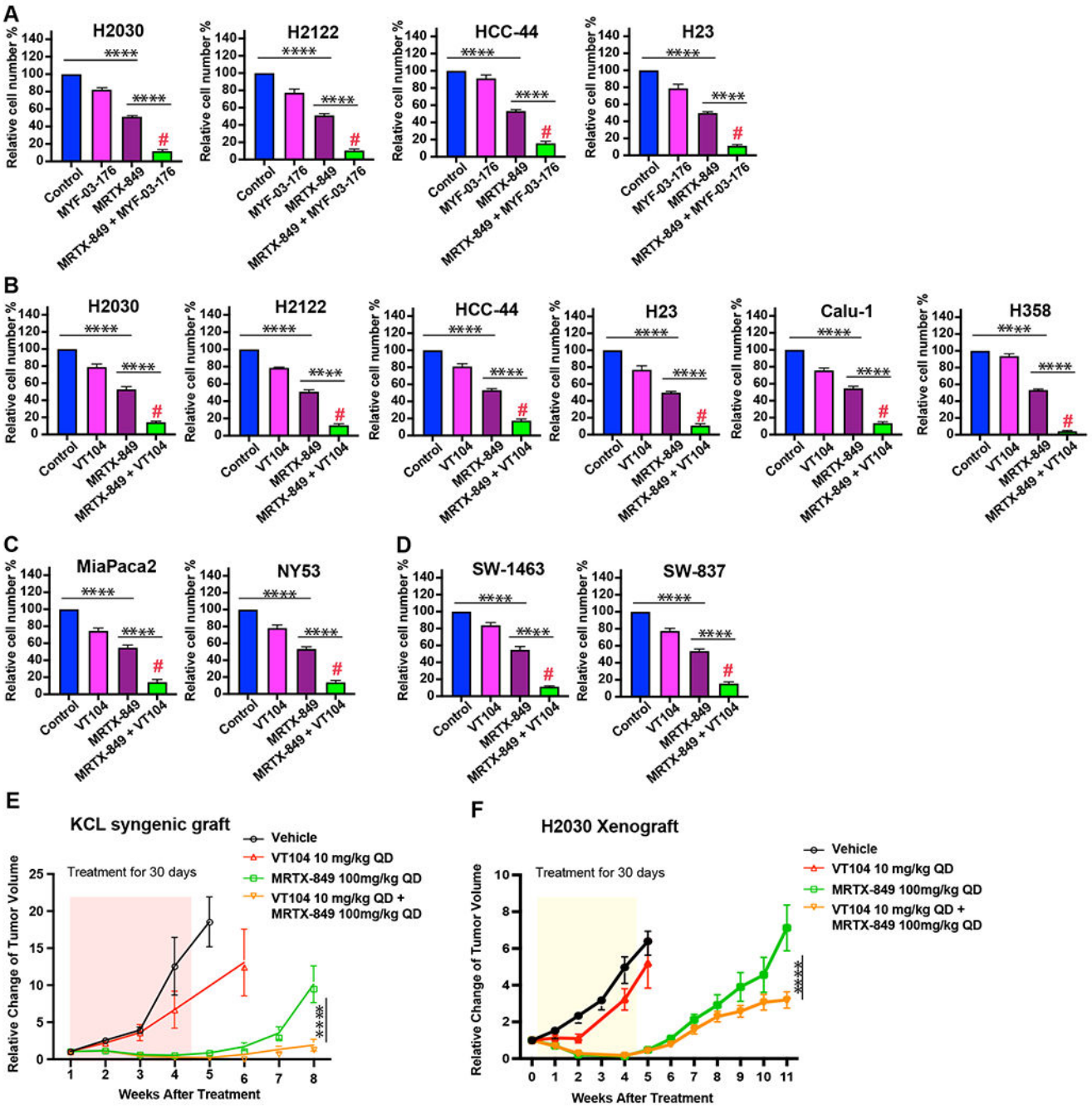

Figure 5. TEAD inhibition enhances efficacy of MRTX-849 in KRAS^{G12C}-mutant cancers.

A, Trypan blue-based proliferation assays (6 days) on H2122, H2030, HCC-44, and H23 lines treated with MYF-03–176 (1μM) and MRTX-849 (at IC50 for each line) alone or in combination. ****p<0.0001, 1-way ANOVA and Tukey's multiple comparisons test **B-D,** Proliferation assays on the indicated cell lines using VT104 (1μM) and MRTX-849 (at IC50 for each line) alone or in combination, ****p<0.0001, 1-way ANOVA and Tukey's multiple comparisons test, #synergy by Bliss independent analysis. **E-F,** Relative change in tumor volumes after withdrawal of treatments at Day 30, *p <0.0001, 2-way ANOVA.

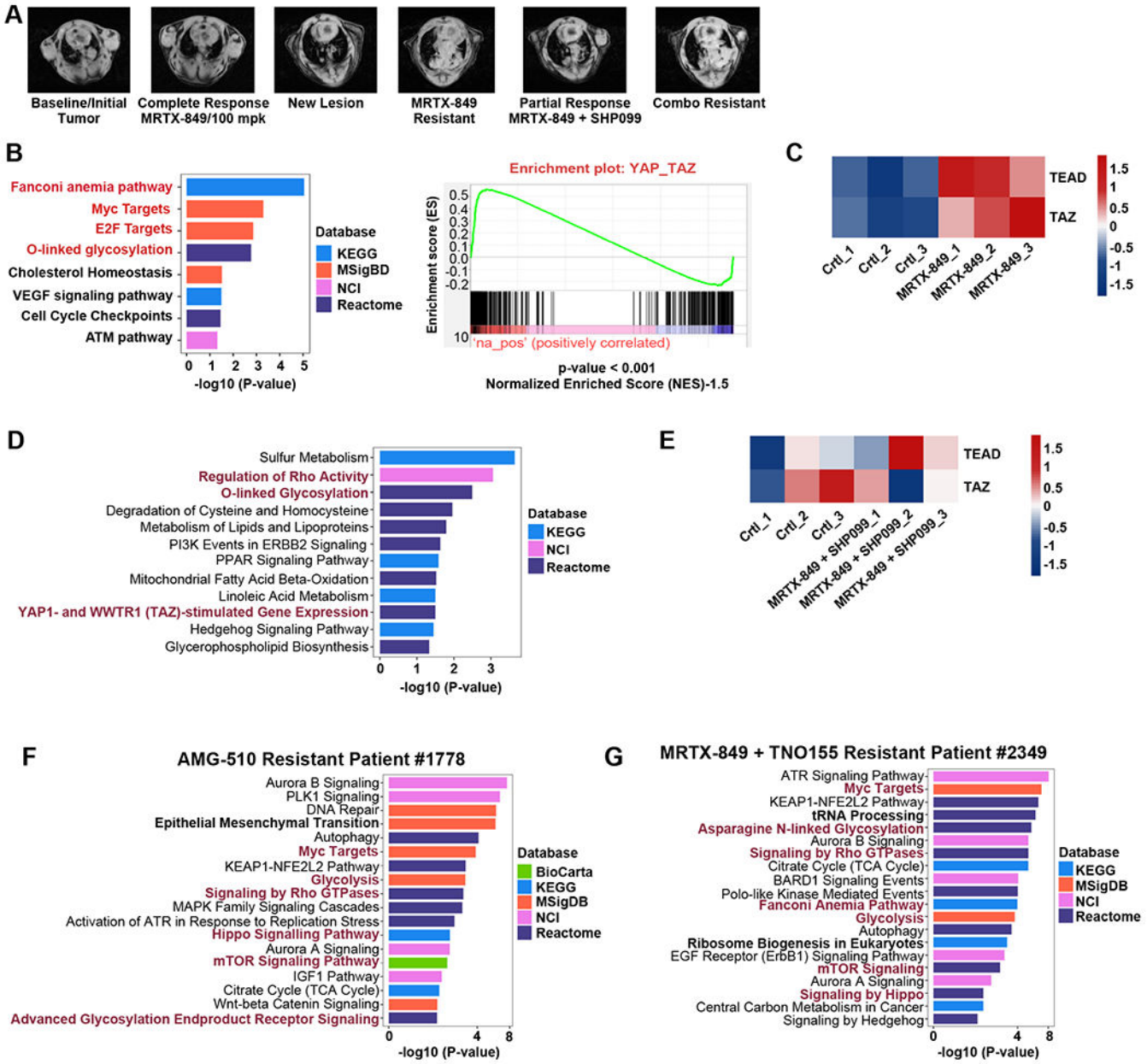

Figure 6. G12Ci- and G12Ci/SHP2 inhibitor-resistant GEMM and patient samples induce pathways overlapping with SL genes:

A, Representative MRI images of KCL mice showing successive development of MTRX-849 and MRTX-849/SHP099 resistance **B, (**Left) Select enriched pathways (p< 0.05) for genes upregulated in MRTX-849-resistant KCL tumors (FDR < 0.1), (Right) GSEA demonstrating increased expression of YAP-TAZ signature genes in these tumors. **C,** Snapshot of RPPA showing increased YAP/TAZ levels in MRTX-849-resistant nodules; see also Supplementary Table S7. **D, (**Left) Select enriched pathways (p< 0.05) for genes upregulated in MRTX-849/SHP099-resistant KCL tumors (FDR < 0.1). (Right) GSEA demonstrating increased expression of YAP-TAZ signature genes in these tumors. **E,** Snapshot of RPPA showing increased YAP/TAZ levels in MRTX-849/SHP099-resistant

nodules; see also Supplementary Table S9. **F-G,** Pathway analysis on sc-RNAseq of cells from fresh tumor biopsies of patients with G12Ci (AMG510)- or G12C/SHP2i (MRTX-849 +TNO155)-resistant NSCLC, as indicated.

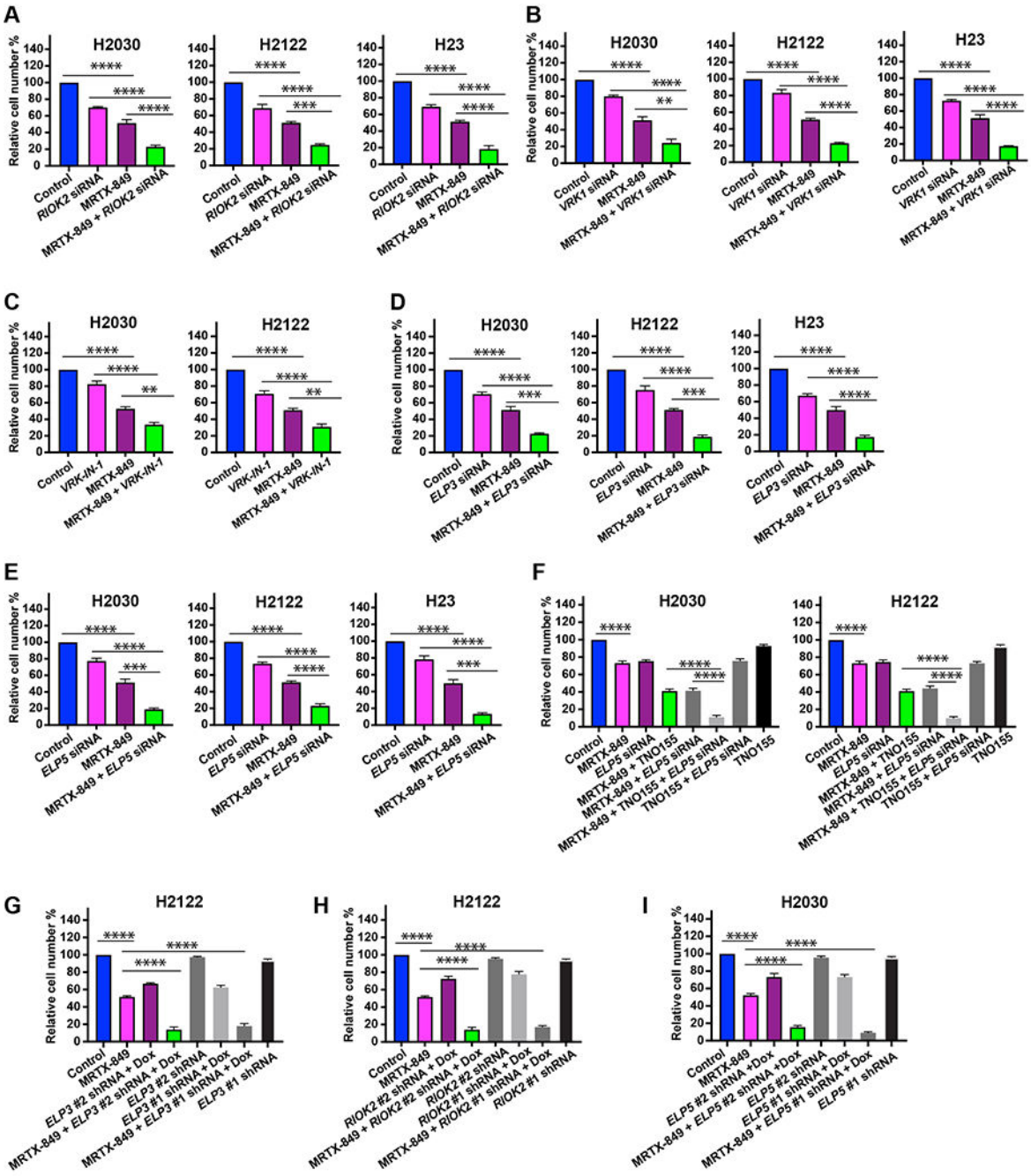

Figure 7. Validation of selected additional targets from screens:

A-B, Trypan blue-based proliferation assays (5-days) on H2030, H2122, and H23 cells transfected with *RIOK2*, *VRK1*, or scrambled siRNAs and/or treated with MRTX-849 (at IC50), as indicated. ****p<0.0001, ***p<0.001, **p<0.01, 1-way ANOVA and Tukey's multiple comparisons test **C,** Trypan blue-based proliferation assays (7 days) on H2030 and H2122 cells treated with VRK-IN-1 (10 μM) and/or MRTX-849 (at IC50), as indicated. ****p<0.0001, ***p<0.001, **p<0.01, 1-way ANOVA and Tukey's multiple comparisons test **D-E,** Same as **A-B**, but with *ELP3*, *ELP5*, or scrambled siRNAs, as indicated. **F,** Trypan

blue-based proliferation assays on H2030 and H2122 cells transfected with scrambled or *ELP5* siRNAs and treated with MRTX-849 and/or TNO155 (at IC25 of each drug in each line) as indicated. ****p<0.0001, ***p<0.001, **p<0.01, 1-way ANOVA and Tukey's multiple comparisons test, **G-I,** Trypan blue-based proliferation assays on H2122 or H2030 cells stably transduced with doxycycline-inducible *ELP3, RIOK2*, *ELP5,* or control shRNA or control shRNA, exposed to Dox for 96 h, and treated with MRTX-849 (at IC50 for each line), as indicated, ****p<0.0001, 1-way ANOVA and Tukey's multiple comparisons test